BAMS Article

A Global Drought and Flood Catalogue from 1950 to 2016

Xiaogang He, Ming Pan, Zhongwang Wei, Eric F. Wood, and Justin Sheffield

ABSTRACT: Hydrological extremes, in the form of droughts and floods, have impacts on a wide range of sectors including water availability, food security, and energy production. Given continuing large impacts of droughts and floods and the expectation for significant regional changes projected in the future, there is an urgent need to provide estimates of past events and their future risk, globally. However, current estimates of hydrological extremes are not robust and accurate enough, due to lack of long-term data records, standardized methods for event identification, geographical inconsistencies, and data uncertainties. To tackle these challenges, this article presents the development of the first Global Drought and Flood Catalogue (GDFC) for 1950–2016 by merging the latest in situ and remote sensing datasets with state-of-the-art land surface and hydrodynamic modeling to provide a continuous and consistent estimate of the terrestrial water cycle and its extremes. This GDFC also includes an unprecedented level of detailed analysis of drought and large-scale flood events using univariate and multivariate risk assessment frameworks, which incorporates regional spatial–temporal characteristics (i.e., duration, spatial extent, severity) and global hazard maps for different return periods. This Catalogue forms a basis for analyzing the changing risk of droughts and floods and can underscore national and international climate change assessments and provide a key reference for climate change studies and climate model evaluations. It also contributes to the growing interests in multivariate and compounding risk analysis.

https://doi.org/10.1175/BAMS-D-18-0269.1
Corresponding author: Xiaogang He, hexg@princeton.edu
Supplemental material: https://doi.org/10.1175/BAMS-D-18-0269.2

In final form 23 December 2019

AFFILIATIONS: He—Department of Civil and Environmental Engineering, Princeton University, Princeton, New Jersey, and Water in the West, Woods Institute for the Environment, Stanford University, Stanford, California; **Pan and Wood**—Department of Civil and Environmental Engineering, Princeton University, Princeton, New Jersey; **Wei**—School of Atmospheric Sciences, Sun Yat-sen University, Guangzhou, China, and Department of Civil Engineering, The University of Tokyo, Tokyo, Japan; **Sheffield**—Department of Civil and Environmental Engineering, Princeton University, Princeton, New Jersey, and Geography and Environment, University of Southampton, Southampton, United Kingdom

Droughts and floods are two extremes of the hydrological spectrum and have a wide range of societal impacts. Historically, droughts and floods have cost $596 billion (U.S. dollars) in damages in the early twenty-first century (2000–17) (EM-DAT 2018) and have affected more than 3.4 billion people during 1995–2015 (UNISDR 2015). Besides these direct costs, impacts can propagate into other sectors due to losses of ecosystem services (e.g., Palmer et al. 2009; Mora et al. 2018), disruption of global supply chains (e.g., Haraguchi and Lall 2015; in den Bäumen et al. 2015; Cottrell et al. 2019), and increased risk mitigation costs (e.g., Kreibich et al. 2017). There is also a growing body of literature exploring the effects of droughts and floods on human health (e.g., Hajat et al. 2005; Haines et al. 2006; Fernandez et al. 2015; Evans 2019), migration (e.g., Perch-Nielsen et al. 2008; Feng et al. 2010; Black et al. 2011; Abel et al. 2019), and conflicts (e.g., Gleick 2014; Maystadt and Ecker 2014; Kelley et al. 2015; Ghimire et al. 2015), although there is as yet no consensus on the causal linkages between these hydrological extremes and their impacts due to the complexity of physical and socioecological systems (e.g., Hajat et al. 2005; Adams et al. 2018; Mach et al. 2019). Nevertheless, these studies highlight the societal value of an improved assessment of drought and flood risk, whose impacts may further increase as a result of climate change and economic development. Evidence from climate model projections shows that climate change will lead to increased frequency and intensity of droughts (e.g., Sheffield and Wood 2008b; Orlowsky and Seneviratne 2013; Trenberth et al. 2014) and floods (e.g., Milly et al. 2002; Pall et al. 2011; Field 2012; Hirabayashi et al. 2013; Arnell and Gosling 2016) at regional scales. This poses serious challenges to mitigation and adaptation strategies as defined in recent global (IPCC 2018), continental (e.g., the Fourth National Climate Assessment; Wuebbles et al. 2017), and regional (e.g., California's Fourth Climate Change Assessment) assessment reports.

To this end, there is a need to improve our understanding of current drought and flood risks and how they may change in the future under the influence of climate change and human activities. However, observational hydrological data from, for example, precipitation and streamflow gauges are sparse over many parts of the world, are often short term, and usually impacted by anthropogenic influences. Consequently, current drought and flood risk estimates are often short term and inconsistent, limited to developed nations, and are often associated with large uncertainties (Seneviratne et al. 2012). Addressing these challenges requires developing a Catalogue of hydrological extremes and their characteristics, which should have long-term data records to enable more robust risk quantification than existing short-term global drought (e.g., Heim and Brewer 2012; AghaKouchak and Nakhjiri 2012; Hao et al. 2014), flood (e.g., Herold et al. 2011; Ward et al. 2013; Brakenridge 2019) and inundation (Pappenberger et al. 2012; Fluet-Chouinard et al. 2015; Ji et al. 2018) products. It also needs to be spatially and temporally continuous and consistent, so that risk can be quantified globally, not only for developed regions [e.g., see recent U.S. flood events compiled by Shen et al. (2017) and European drought Catalogue by Lloyd-Hughes et al. (2009)] but also for data-poor regions (such as much of Africa). Moreover, drought and flood risk should be quantified in a consistent way to enable a comprehensive understanding of both extremes to improve risk

assessment and water resources management that can further mitigate impacts. As droughts and floods share the same types of interlinked characteristics (e.g., severity, area, duration), and potentially linked driving mechanisms, their cooccurrence could contribute to even larger impacts than the sum of each individual type of extreme because of the exacerbation of human vulnerabilities (e.g., King-Okumu et al. 2018). Therefore, dependence structures between the contributing variables should be well represented to avoid the underestimation of the compounding impact that can occur if risk is assessed based on the traditional univariate frameworks, which only focus on a single variable (Zscheischler and Seneviratne 2017; Moftakhari et al. 2017; Hao et al. 2018). In fact, a multivariate risk assessment framework has the advantage to simultaneously consider the interlinkages between different impact-contributing factors (e.g., event characteristics or drivers). It allows us to have a more comprehensive understanding of the combined impact of extremes and therefore has been increasingly recommended by several international guidelines (e.g., European Union 2007).

We are now in a much better position to tackle the above challenges thanks to a series of advancements in monitoring, modeling and risk assessment. This includes recent development in satellite-based hydrological measurements (e.g., Lettenmaier et al. 2015; Sheffield et al. 2018), advances in large-scale land surface and hydrodynamic modeling (e.g., Yamazaki et al. 2011; Bierkens 2015) as well as improved risk quantification and event identification approaches (e.g., Andreadis et al. 2005; Leonard et al. 2014; He et al. 2017; Hao et al. 2018). Leveraging on these advancements, this study aims at developing the first Global Drought and Flood Catalogue (GDFC). The GDFC is generated based on 0.25°, long-term (1950–2016) and improved land surface and river simulations driven by quality-controlled and consistent meteorological forcings. Although there exists other global-scale drought (e.g., Global Drought Information System; Nijssen et al. 2014) and flood (e.g., Dartmouth Flood Observatory; Brakenridge 2019) databases, their short-term data records jeopardize their ability for robust risk quantification. In addition, most of them only focus on one type of extreme (either droughts or floods) and therefore do not provide a joint picture of how droughts and floods evolve together. The GDFC is distinguished from, but also complementary to, existing hazard databases from both the univariate and multivariate perspective, ensuring a global-scale and robust quantification of these hazards. It could also be used as a reference to evaluate other datasets and future changes in droughts and floods.

Overview of approach

The GDFC focuses on droughts and large-scale floods (both pluvial and fluvial). It builds upon legacy systems developed previously at global (Sheffield and Wood 2007, 2008a) and regional (Sheffield et al. 2014) scales, making use of existing models and datasets, but has been enhanced in the following aspects to provide better estimates of the global terrestrial hydrological cycle and its extremes (Fig. 1). We first extend the existing long-term global meteorological dataset [Princeton Global Forcings (PGF); Sheffield et al. 2006] from 1950 to near present (2016), which is also enhanced in its spatial resolution (0.25°) through statistical downscaling and corrected for temporal and spatial inconsistencies (see details in appendix A, "Enhanced global meteorological forcings" section). This new version (v3) of the PGF is then utilized to drive an updated version of the Variable Infiltration Capacity (VIC) land surface model (see appendix A, "Enhanced land surface model simulations" section, for details) to obtain an improved estimate of soil moisture and runoff variability that is key to understanding changes in drought and flood (pluvial and fluvial) risk. We also implement a newly developed global-routing and hydrodynamic model Catchment-Based Macro-Scale Floodplain model (CaMa-Flood) to explicitly characterize flood stage (e.g., inundation area and water level) and river discharge (see appendix A, "Enhanced routing model" section, for model details and Fig. S1 in the online supplemental material for streamflow validation results; https://doi.

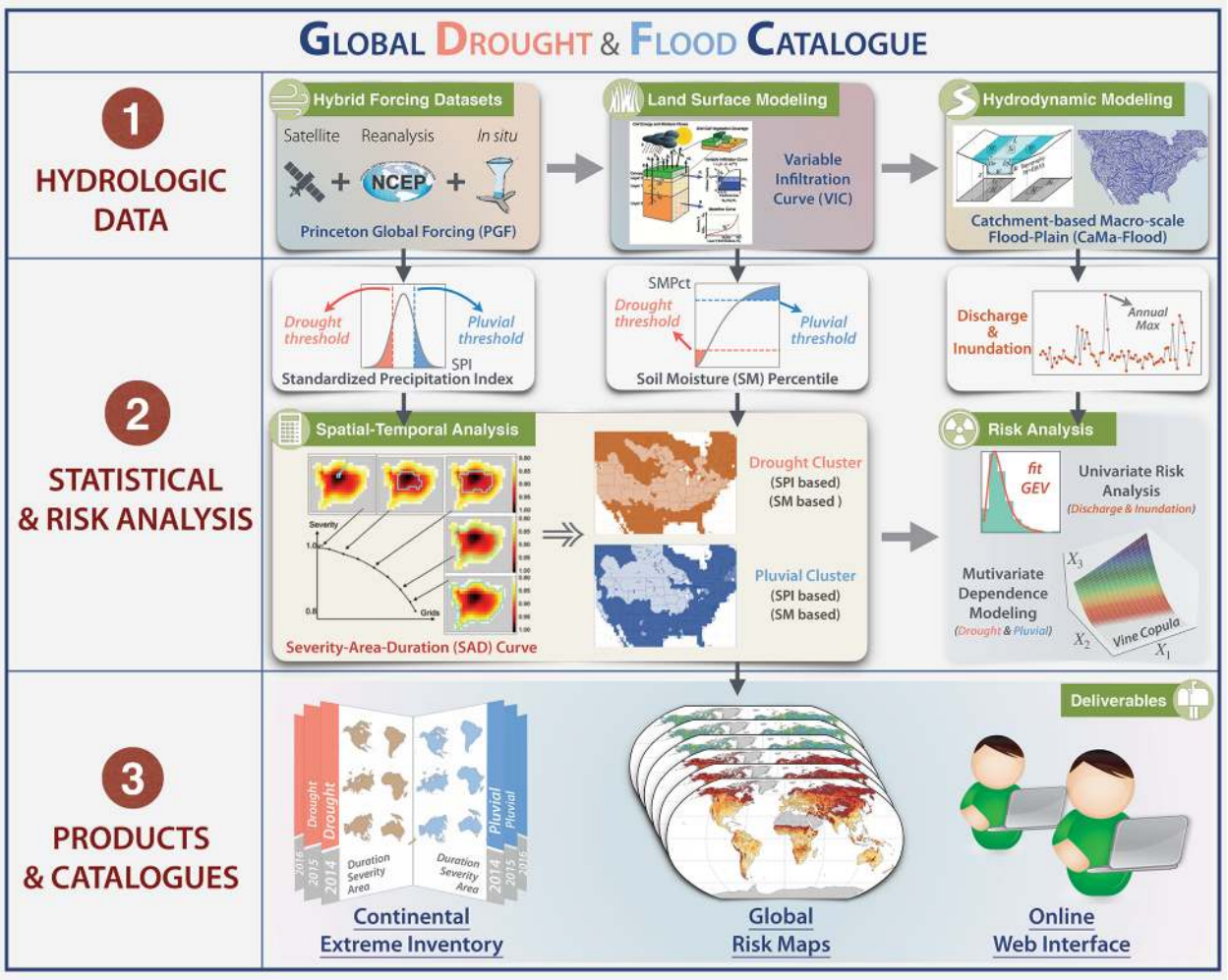

Fig. 1. Schematic of the overall framework illustrating three major steps to develop the Global Drought and Flood Catalogue (GDFC). Step 1 is generating long-term and consistent hydrologic datasets using state-of-the-art physically based hydrologic modeling platform that includes hybrid meteorological forcings (PGFv3), improved land surface modeling (VIC), and enhanced hydrodynamic model (CaMa-Flood). Step 2 is robust quantification of drought and flood/pluvial risk based on a suite of statistical postprocessing procedures, including the statistical transformation of hydrologic data into standardized indices for drought and large-scale flood identification, spatial and temporal clustering analysis, univariate risk analysis, and multivariate dependence modeling. Step 3 is developing a meta-database to deliver products and Catalogues (e.g., drought and pluvial inventory at the continental scale, global risk maps for different types of hydrological extremes, and an online web interface) that enables dissemination of knowledge and data to the wider scientific community.

org/10.1175/BAMS-D-18-0269.2). Related hydrological variables (e.g., 3-month accumulative precipitation from the PGFv3 and monthly soil moisture simulated from VIC) are then transformed to standardized indices (see appendix B, "Standardized indices" section) to identify drought and pluvial events at the pixel level based on run theory (appendix B, "Run theory to estimate drought and pluvial (defined as large-scale and long-term wet extreme) frequency" section). Given the dynamic nature of hydrologic extremes, a joint spatial–temporal analysis is performed to investigate how droughts and pluvials propagate, merge (two events merging into one) or break up (an event splitting into two or more events separated in space) through time and space. We utilize a severity–area–duration (SAD) clustering algorithm (appendix B, "Clustering algorithm for drought and pluvial identification" section) to identify spatially contiguous drought and pluvial events over six continents (excluding Antarctica) and examine

the stationarity of their evolution through the estimation of their time-varying frequency (see appendix B, "Stationarity of drought and pluvial events" section, for details). Characteristics (i.e., frequency, spatial extent, severity) of drought and pluvial events (and their associated flooding) are synthesized into a Catalogue with a particular focus on characterizing the long-term variability in risk from both a univariate and multivariate perspective (appendix B, "Copula-based risk analysis" section).

Deliverables

To enable dissemination of knowledge and data to the wider scientific community and enable feedback, a publicly accessible Internet data portal and web interface (http://hydrology.princeton.edu/data/hexg/GDFC/) has been developed. This delivers relevant products, including continental drought and pluvial Catalogues, global-scale drought and flood (pluvial and fluvial) risk maps, long-term meteorological and agricultural standardized indices, the underlying meteorological forcings, and land surface hydrological fluxes and states (Table 1), which can be used to underpin climate services (e.g., Hewitt et al. 2012; Goddard 2016; Haigh et al. 2018). More specifically, these datasets could be utilized by the humanitarian community, development funding agencies and insurance companies for risk analysis, investment planning, and targeted early warning especially over developing countries (e.g., in Africa) with sparse data and low coping capacities.

Results

Stationarity and trend of spatially contiguous drought and pluvial frequency. Acknowledging the dynamic nature of droughts and pluvials and their interrelated characteristics (e.g., severity, area, and duration), it is necessary to investigate their variation and trends at

Table 1. Data products included in the Global Drought and Flood Catalogue.

Products	Types/variables/indices	Data source and description	Attributes	Format
Catalogue	Drought inventory (agricultural and meteorological)	SAD clustering algorithm	Event ID, date, duration, spatial extent, severity (six continents)	txt, csv
	Pluvial inventory (agricultural and meteorological)			
Hazard maps	Drought frequency (agricultural and meteorological)	Return period calculated from standardized indices	0.25°; duration with 1–3, 4–6, 7–12, and >12 months	netCDF4
	Pluvial frequency (agricultural and meteorological)			
	Fluvial risk maps	Annual maximum inundation fraction and daily streamflow estimated from CaMa-Flood simulations and GEV distribution	0.25°; 5-, 10-, 20-, 50-, 75-, 100-, 200-, and 500-yr return periods	
Standardized indices	Standardized precipitation index	Precipitation from PGFv3 (1950–2016)	0.25°; SPI1, SPI3, SPI6, SPI12; daily, monthly, yearly	netCDF4
	Soil moisture percentile	VIC land surface model (1950–2016)	0.25°; daily, monthly, yearly	
Meteorological forcings	Precipitation, 2-m temperature, downward surface shortwave radiation, downward surface longwave radiation, 2-m specific humidity, surface pressure, 10-m wind	PGFv3 (1948–2016)	0.25°; 3-hourly, daily, monthly, yearly	netCDF4
Land surface hydrological fluxes and states	Evapotranspiration, runoff, soil moisture at different layers (0.1 and 1 m), streamflow, inundation area and fraction	VIC land surface model and CaMa-Flood hydrodynamic model (1950–2016)	0.25°; daily, monthly, yearly	netCDF4

the event level. We count the occurrence of spatially contiguous droughts and pluvials using the SAD technique and examine the stationarity of event frequency based on time-varying occurrence rate and associated long-term trends through a nonparametric Gaussian kernel (Fig. 2). Globally, there are 453 and 476 short-duration meteorological droughts and pluvials, respectively, with a contiguous area larger than 375,000 km^2 from 1950 to 2016. Fewer (200) medium-duration events are identified, indicating that prolonged hydrological extremes have less persistence and tend to break into short-term events during their evolution. This is also evidenced by the soil moisture percentile (SMPct)-based analysis with a reduced number (179)

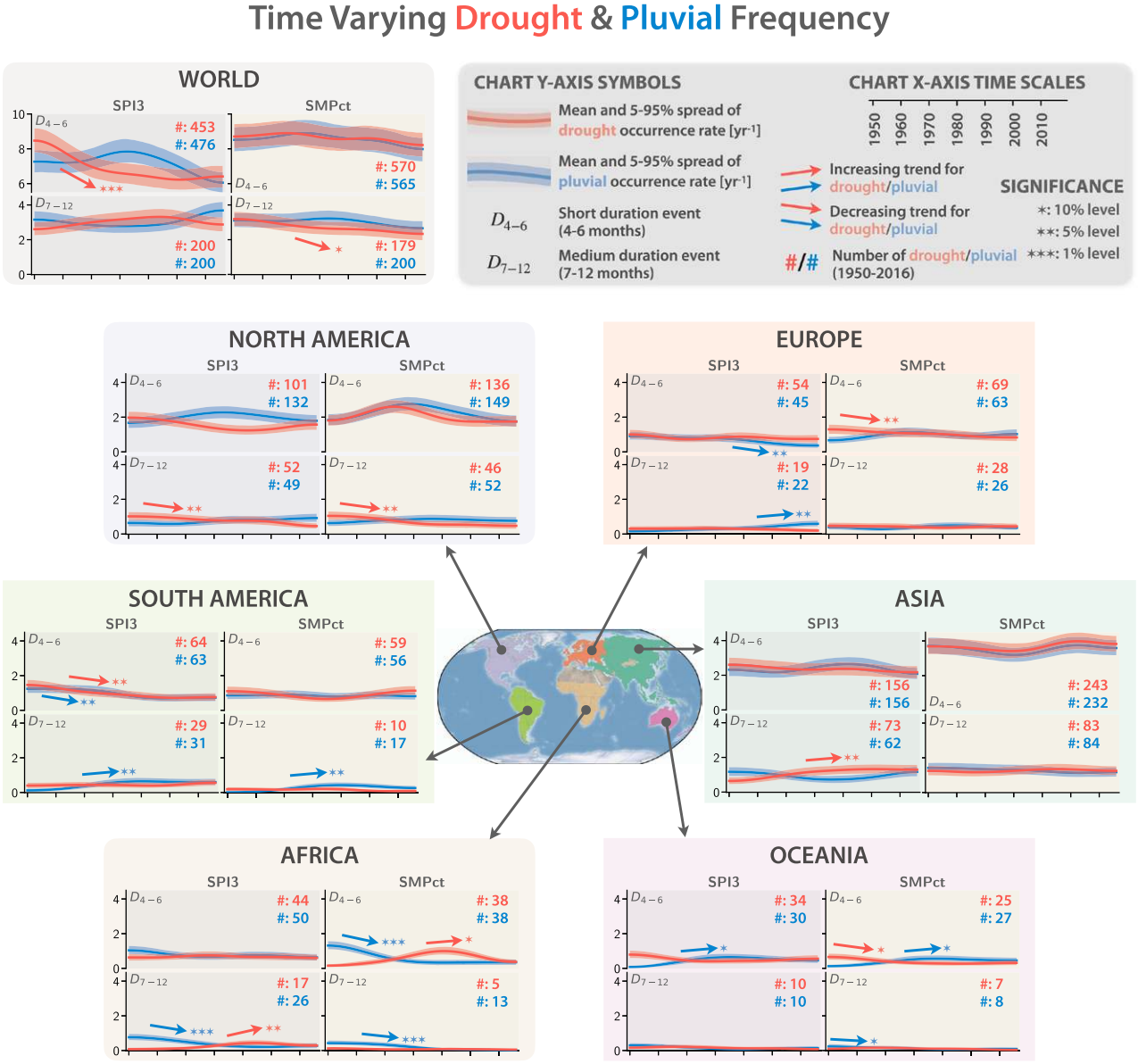

Fig. 2. Time-varying occurrence rates (yr^{-1}; bold lines) and 90% confidence bands (shaded area) for spatially contiguous short-duration ($D_{4–6}$, 4–6 months) and medium-duration ($D_{7–12}$, 7–12 months) drought (red color) and pluvial (blue color) events during 1950–2016 identified through the SAD clustering approach using the 3-month standardized precipitation index (SPI3; left side of each panel) and soil moisture percentile (SMPct; right side of each panel). The upward and downward arrows in each panel indicate statistically significantly increasing and decreasing trends, respectively, based on different levels of significance (represented by different numbers of stars). We divide the global land surface (excluding Greenland and Antarctica) into six continents (i.e., North America, Europe, South America, Asia, Africa, and Oceania) based on Sheffield et al. (2009) and mask out extremely dry regions with annual rainfall less than 100 mm.

of medium-duration droughts and consequently an increased number of short-term droughts (570). Among the six continents, Asia has the largest number of occurrences of both short- and medium-duration droughts and pluvials, followed by North America, whereas Oceania has the smallest number. This is mainly due to the domain size.

For meteorological extremes [based on 3-month standardized precipitation index (SPI3)], globally the frequency of short-term droughts has decreased significantly ($p < 0.01$), from more than eight events per year in the 1950s to roughly six events per year in the 1990s, and then stabilizes afterward. There is no statistically significant trend in short-term pluvial frequency over the whole study period, but it increases slightly in the first half of the study period and decreases dramatically in the second half, with peak occurrence rate around eight times per year during the 1980s. Such an out-of-phase relationship in the long-term trend between short-term droughts and pluvials is also shown in other continents, including North America and Asia, although the decadal fluctuation in event frequency has been dampened due to the large size of the region. Short-term meteorological droughts occur less frequently ($p < 0.05$) in recent decades over South America, which is consistent with the decreased probability of dry extremes over northeastern South America (Schubert et al. 2016). In contrast, short-term meteorological pluvials have a slightly increasing trend over Oceania, although with a reduced degree of statistical significance ($p < 0.1$). For medium-duration events, droughts and pluvials occur roughly half as frequently as short-term events and with reduced decadal variability. We observe that the occurrence of medium-duration pluvials has become more frequent in recent decades over Europe and South America ($p < 0.05$), whereas medium-duration droughts occur more frequently over Asia ($p < 0.05$). Over Africa, the robust increasing trend of medium-duration drought occurrence is coincident with the decreased frequency in medium-duration pluvials. This is consistent with previous findings arguing that Africa is moving toward a drier climate at regional (Liebmann et al. 2014; Diem et al. 2014) and continental (Dai et al. 2004b; Dai 2011) scales.

The soil moisture–based analysis illustrates a complementary picture of drought and pluvial occurrence. Compared to the SPI3-based analysis, frequency estimation using SMPct shows an overall reduced decadal variability and a more synchronous and coherent temporal evolution between droughts and pluvials, as reflected at both global and regional scales. However, over Africa and Oceania, we find opposite temporal trends between short-duration droughts and pluvials, with a robust decreasing trend in one extreme contemporaneous with robust increasing frequency of the other. Such patterns over Africa show the vulnerability of this region to both dry and wet extremes, due to the high variability in soil moisture that is partly influenced by the intertropical convergence zone (ITCZ) seasonal footprint (Sheffield and Wood 2007). Oceania experiences a wetting trend in soil moisture, resulting in more frequent pluvials and less frequent droughts (Sheffield and Wood 2008a). We also find that, at the global scale, the frequency of short-duration extremes has significantly higher magnitude estimated from SMPct compared to that estimated from SPI3, which is mainly attributed to the difference in Asia and North America. Regardless of what event index is used, the estimated trends are consistent between SPI3 and SMPct for medium-duration droughts over North America, medium-duration pluvials over South America and Africa, and short-duration pluvials over Oceania. This highlights the dominant role of changing precipitation that leads to more frequent meteorological extremes and can translate to agricultural extremes through the filtering of land surface hydrologic processes. For regions lacking such consistency between SPI3 and SMPct, the complexity of hydrologic processes (e.g., soil moisture memory effects, snow processes, land–atmosphere coupling) and how they respond to long-term changes in precipitation needs further investigation to improve our understanding of drought and pluvial occurrence. In summary, the detected trends of drought and pluvial frequency are geographically variable and may not be consistent or

statistically robust depending on what index is used. Frequency differences between short- and medium-duration extremes highlight the need to improve our understanding of how prolonged events persist or break up under changing atmospheric conditions and changing hydrological processes, such as local land–atmospheric feedbacks (Guillod et al. 2015; Miralles et al. 2019) and large-scale teleconnections with sea surface temperatures (Pal and Eltahir 2002; Wang et al. 2015; Sheffield et al. 2009) that may lead to self-intensification and self-propagation of extreme events.

Continental inventory of drought and pluvial episodes. **SAD ANALYSIS OF CONTINENTAL DROUGHTS AND PLUVIALS.** Figure 3 shows all agricultural drought and pluvial events with a 3-month duration. For small-area extent, SAD curves overlap with each other, because different events tend to have similar severity (these are usually localized events). As fraction of total area of the continent increases, the SAD curves start to diverge, which is due to the increased spatial variability of soil moisture as drought expands to a larger area. Out of the six continents, droughts and pluvials identified in Asia generally have smaller fractions of spatial coverage (less than 20%), but the absolute area could be large given the domain size. In contrast, extremes that occurred in Oceania usually cover a much larger area (e.g., the maximum spatial coverage can be more than 80% of the total area). The reduced number of occurrences in this region is largely due to the small domain size, and the SAD curves are more dispersed compared to other regions. These findings also hold true for SPI3-based analysis (Fig. S2). As expected, longer-duration events (6 and 9 months) are rarer (fewer lines in Figs. S3–S6). However, these longer-duration events move and propagate to other places and therefore become more spatially extensive (e.g., maximum fraction area in Figs. S5 and S6 is larger than that in Fig. 3 and Fig. S2).

To further explore the relationship between droughts and pluvials, we slice the 2D SAD curves (Fig. 3 for example) within a certain window (horizontal or vertical) and calculate the cumulative distribution function (CDF) conditioned upon area and severity for both

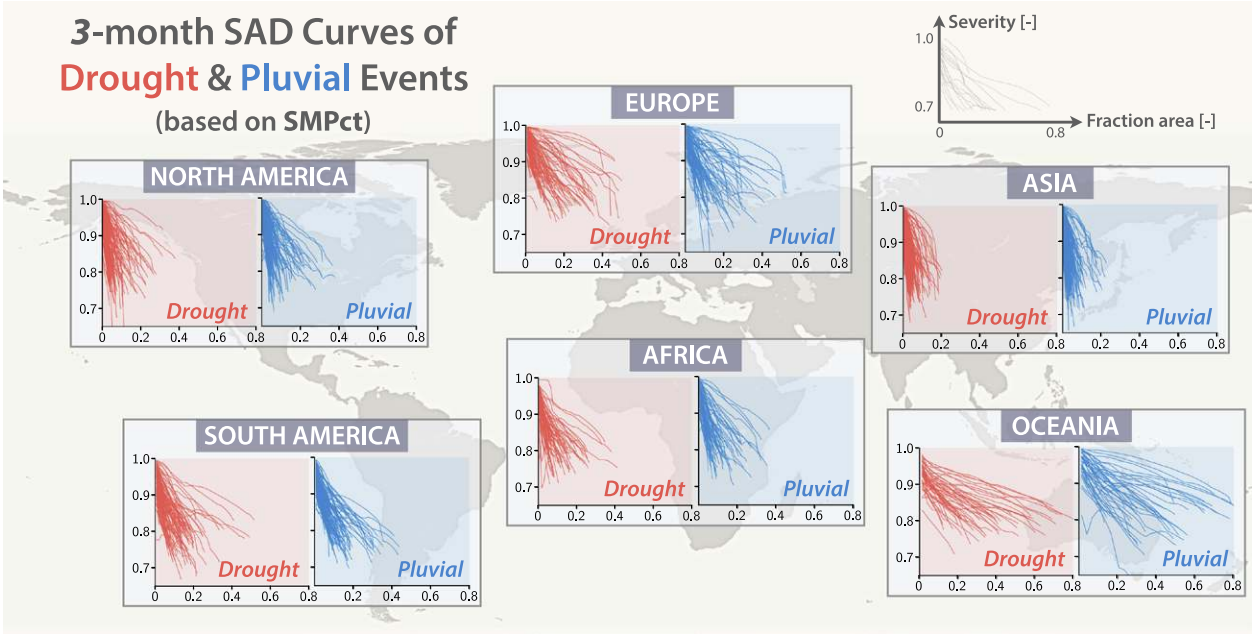

Fig. 3. SAD curves showing the relationship between severity and spatial extent (represented by fraction area) for 3-month droughts (left side of each panel) and pluvials (right side of each panel) based on SMPct. Each line represents a specific event that is spatially contiguous given the specified duration (3 months here). Severity decreases as droughts and pluvials expand to a larger area.

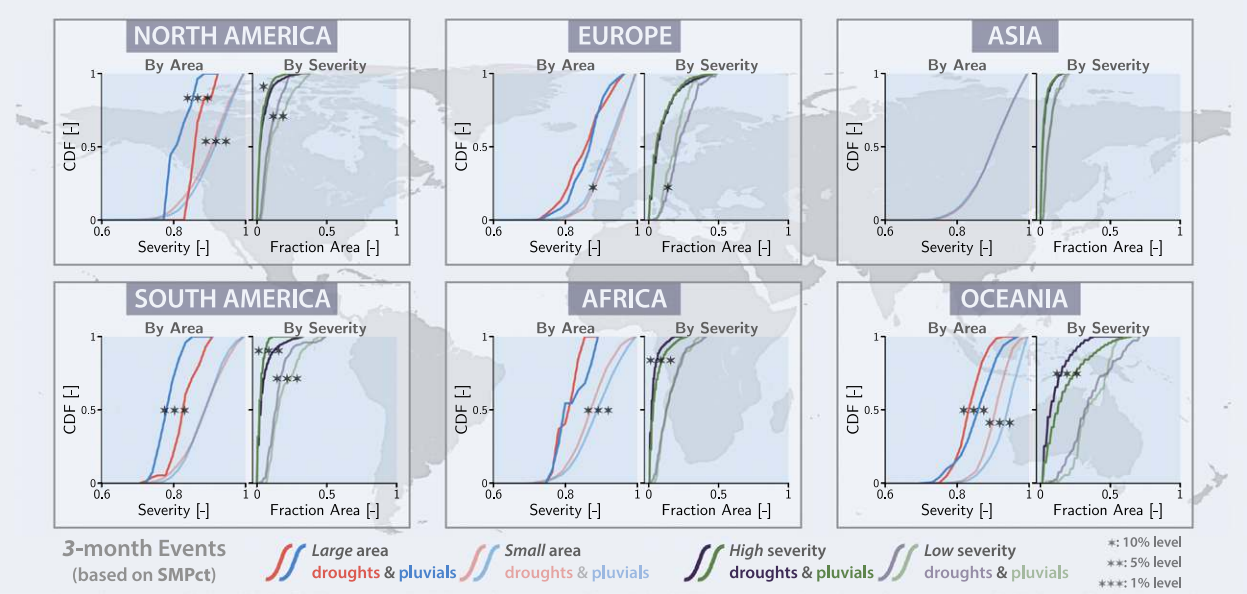

Fig. 4. Comparison of the empirical cumulative distribution function (CDF) between the 3-month droughts and pluvials conditioned on area (left side of each panel) and severity (right side of each panel) across six continents using SMPct as the event index. The two-sample K-S test is performed for each pair to examine whether the differences in CDF between droughts and pluvials are statistically significant. The number of stars represents the level of significance.

SMPct- (Fig. 4, Figs. S7 and S8) and SPI3-based index (Figs. S9–S11). We group events into large (fraction area ≥ 30%) and small (fraction area ≤ 10%) area as well as high (≥0.9) and low (≤0.8) severity categories. We conduct a two-sample Kolmogorov–Smirnov (K-S) test to examine whether the CDF between droughts and pluvials is statistically significantly different. In North America, results show that large-area pluvials are less severe than large-area droughts, which holds true for both SMPct- and SPI3-based analysis. However, only the SMPct-based results show that smaller-area pluvials are more severe. Moreover, the SMPct-based analysis indicates that low-severity pluvials are usually larger than low-severity droughts. However, from the meteorological perspective (based on SPI3), pluvials usually have smaller spatial extent than droughts (except for the low-severity pluvials with 3-month duration). In Europe, short-duration pluvials tend to be less severe than short-duration droughts (e.g., Fig. S9). For longer-duration events (i.e., 9 months), large agricultural pluvials (Fig. S8) and small meteorological pluvials (Fig. S11) tend to be more severe than droughts. In terms of event size, pluvials are generally smaller than droughts in this region, but the significance level of the difference varies with duration and severity category. In Asia, meteorological pluvials are more severe but slightly smaller compared to meteorological droughts for all durations (Figs. S9–S11). For agricultural extremes, statistical differences between droughts and pluvials are only evident for 9-month-duration event (Fig. S8). For such prolonged events, pluvials tend to be more spatially extensive and severe than droughts. Pluvials that occurred in South America and Africa are less severe than droughts. With a few exceptions (e.g., 3-month low-severity agricultural extremes and 6-month meteorological extremes), pluvials also tend to cover smaller areas than droughts. Oceania pluvials extend to have larger areas than droughts and also tend to be more severe.

Among all the drought and pluvial events, the top five events ranked by duration and spatial extent are summarized in Figs. 5 and 6 and Table S1 for each continent. For agricultural extremes, North America has the longest-duration (97 months) drought lasting from June 1951 to June 1959, which also turns out to be the most spatially extensive one with peak extent covering 83.2% of the total area. For pluvials, the top two longest episodes occurred in Asia (i.e.,

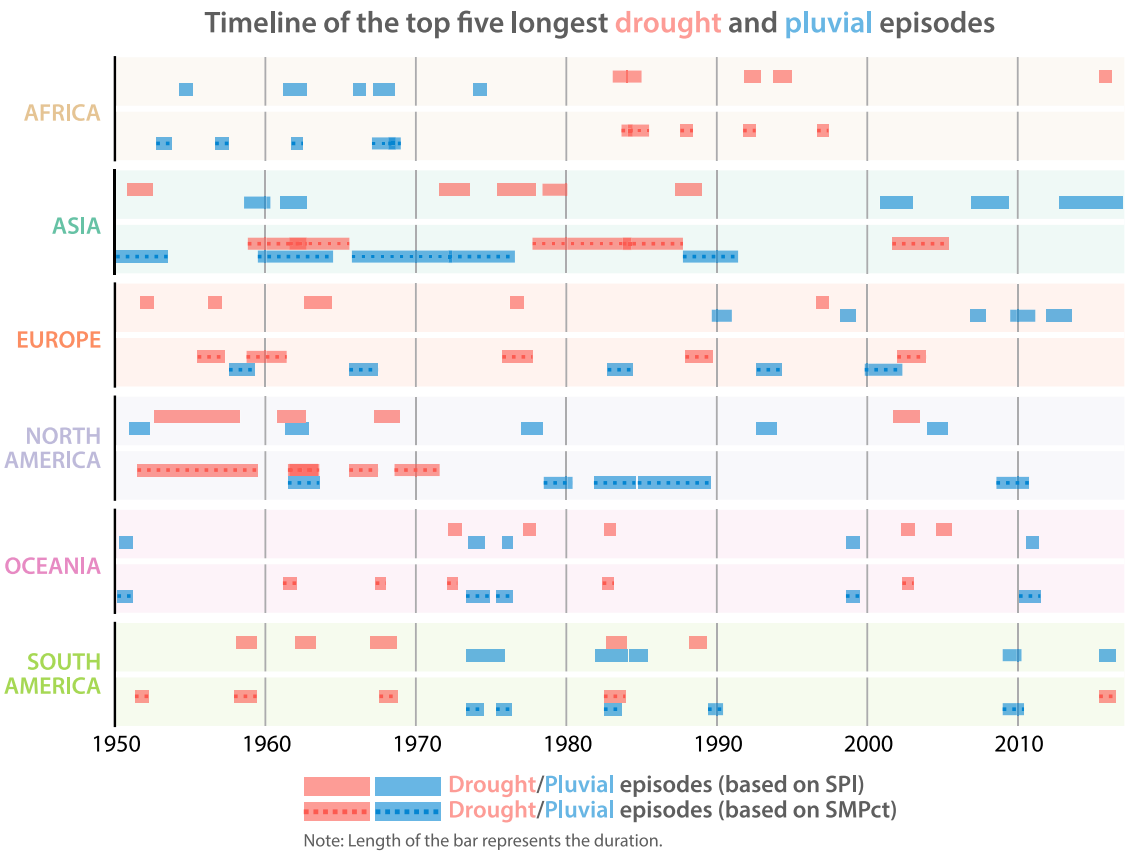

Fig. 5. Timeline of the top five drought (pink color) and pluvial (blue color) episodes ranked by duration. These events are detected by the SAD clustering algorithm using SPI and SMPct. See details in Table S1.

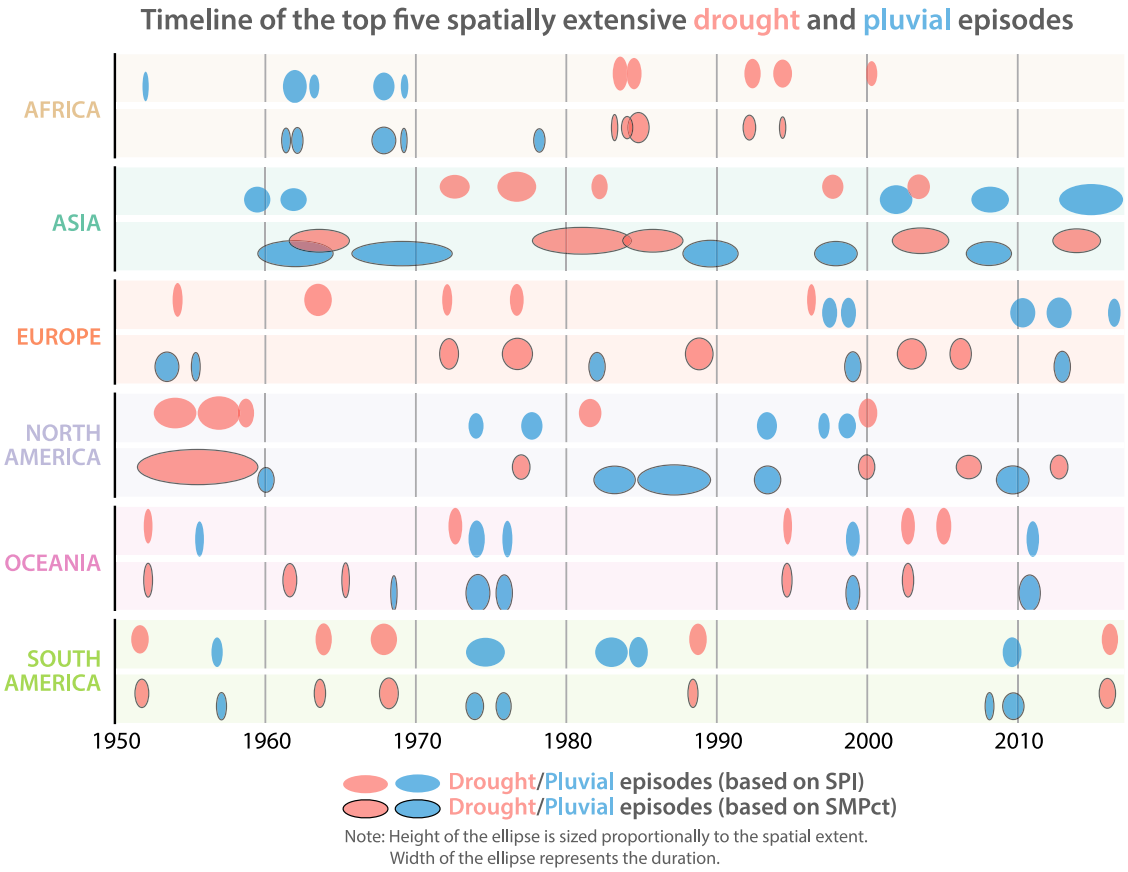

Fig. 6. As in Fig. 5, but events are illustrated based on the rank of the spatial extent.

81 months from 1965 to 1972 and 61 months from 1959 to 1964). The most spatially extensive episode is found in Oceania from April 1973 to November 1974 with the highest coverage up to 92.4%, which also has the longest duration (20 months) over Oceania. For meteorological extremes, droughts with the longest duration again occur over North America with a similar timing (in the 1950s) compared to the SMPct-based results, but with a much shorter duration (35 months). Longer-duration pluvials are mainly found in Asia during more recent decades (after 2000) compared to those long-lasting episodes occurring in earlier periods (from the 1950s to the 1970s) as detected from SMPct. Out of the six continents, Oceania has the largest meteorological droughts and pluvials, which also tend to cover a larger area than agricultural extremes.

Continental SAD envelope curves for droughts and pluvials. Based on all individual SAD curves (e.g., Fig. 3 and Figs. S2–S6), we extract the maximum bound of severities for a given areal fraction to form a set of SAD envelope curves with different durations (Fig. 7 for droughts and Fig. 8 for pluvials based on SMPct). These envelope curves allow us to construct a continental profile of the most severe droughts and pluvials. We find that, for prolonged (i.e., 9-month duration) events, severe droughts tend to have larger spatial extent than severe pluvials for both SMPct- and SPI3-based estimates. For short-duration (3 and 6 months) events, severe droughts have an overall higher severity than severe pluvials for both agricultural (except Africa and Oceania) and meteorological type. Comparison between agricultural and meteorological extremes (Figs. 7 and 8 vs Figs. S12 and S13) indicates that SMPct-based SAD envelope curves tend to be less stretched out compared to SPI3-based envelope curves, especially for short-duration events. This is also true even for smaller-area events, as we can see clear differences in severity across SAD envelope

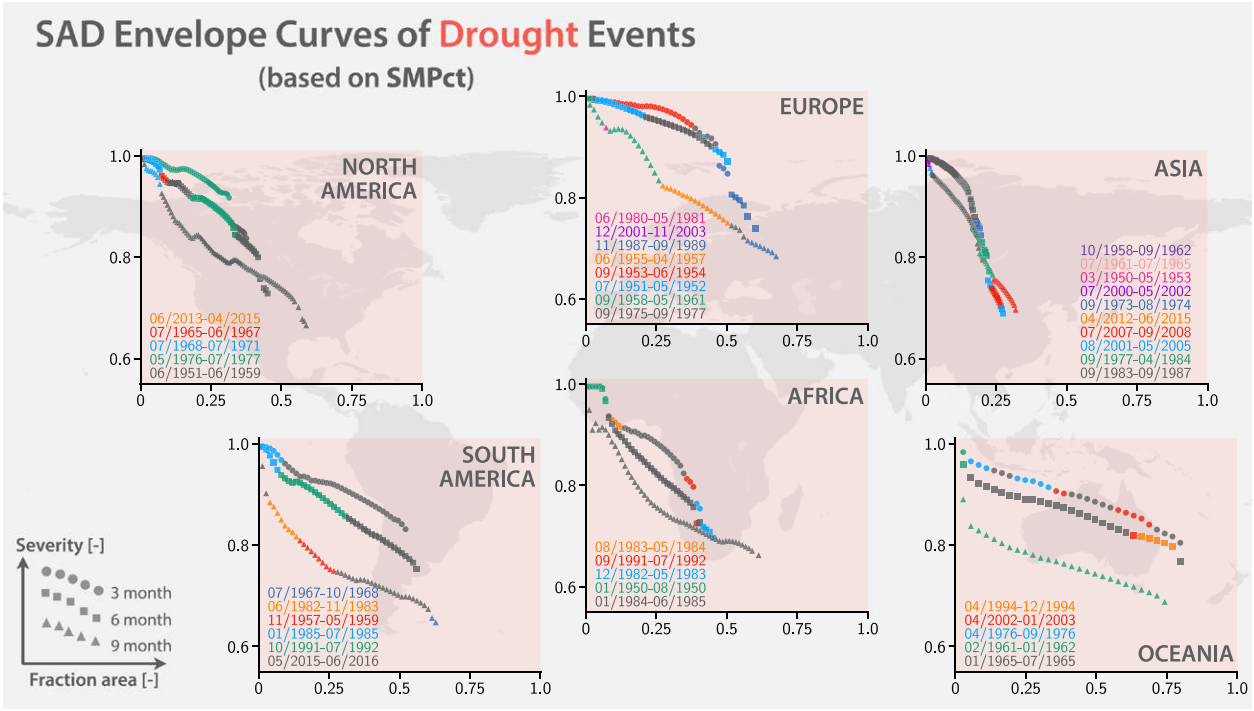

Fig. 7. Continental SAD envelope curves for drought events with different durations (3, 6, and 9 months, represented by different markers). For a particular duration (e.g., 3 months), the curve is generated by selecting the maximum bound of severities from all drought events (e.g., left side of each panel in Fig. 3). Each curve can be made up of different episodes (represented by different colors), as some events are more severe for large areas while others could be more severe for localized events (with smaller areas).

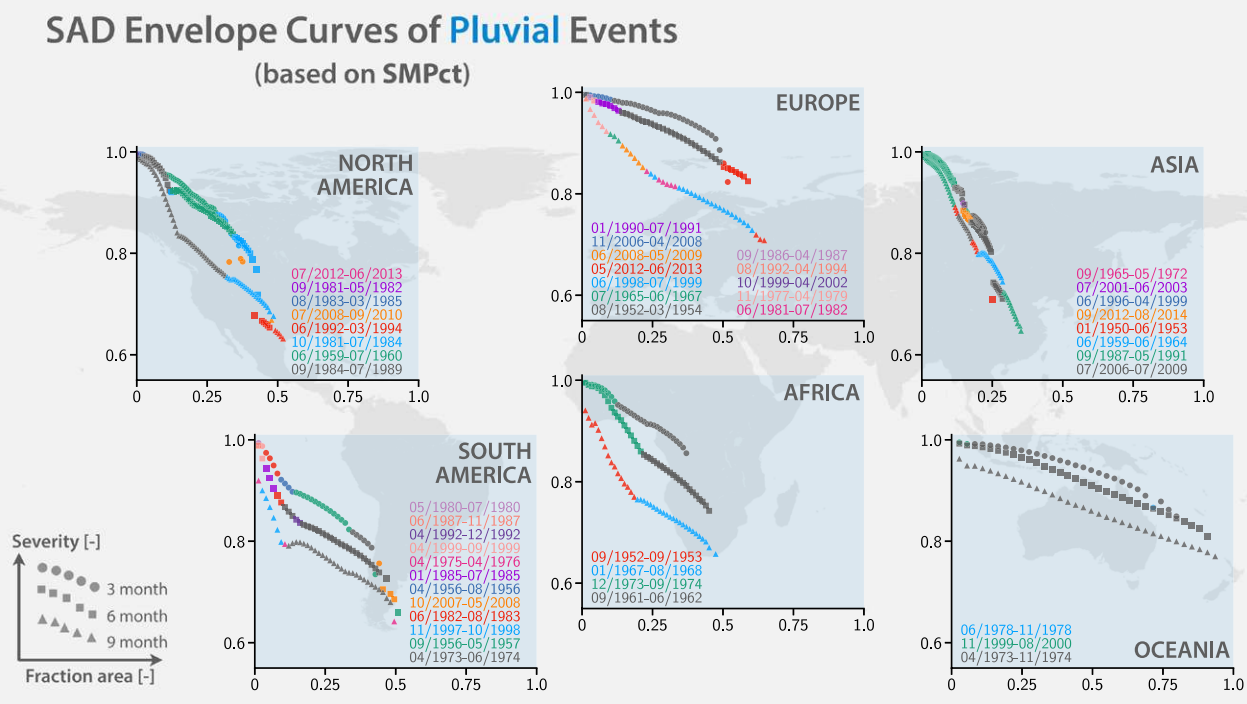

Fig. 8. As in Fig. 7, but for large-scale pluvial events.

curves with different duration. However, the severity of short-duration events tends to overlap with each other based on SMPct. In addition, SPI3-based SAD envelope curves tend to consist of fewer event episodes compared to SMPct, except for droughts in North America and Africa, as well as pluvials in North America and Oceania. This implies that meteorological extremes tend to be dominated by single severe episodes affecting larger areas, whereas agricultural extremes tend to be made up of several severe events that have limited spatial influence and might occur in different periods or regions. In addition, drought and pluvial envelopes estimated from SPI3 have higher severity, larger extent, and shallower slope compared to those based on SMPct, although with a few exceptions (e.g., all events over North America, 9-month droughts over Europe, 3–9-month pluvials over Europe), indicating a lower decreasing rate of severity with increasing area. This further implies that as droughts and pluvials develop, meteorological extremes tend to persist over a larger domain while maintaining a higher severity compared to agricultural extremes. Acknowledging the geographical variations, we discuss major drought and pluvial events for each continent in the following sections.

Meteorological droughts and pluvials. This section documents major droughts and pluvials for each continent from the meteorological perspective (Figs. S12 and S13). In North America, the top two longest droughts (1952–55, 1955–58; see Table S1 and Fig. 5) contribute to the majority of the SAD envelope curves, especially for large fraction of spatial extent. For smaller extent and short duration, drought envelopes are mainly made up from the 1976/77 event. These results are consistent with the depiction of agricultural droughts (Fig. 7) with similar location and spatial coverage. Pluvial envelope curves in this region are steeper compared to drought, and the maximum spatial extent is also reduced. The longest-duration pluvial during the 1960s (1961/62; Table S1) dominates the 9-month envelope curve for smaller extent, whereas the 1990s (1992/93 and 1996/97) pluvials (Seager et al. 2005) dominate envelope curves with larger extent, which also rank the second and third in terms of spatial extent (Table S1 and Fig. 6). Note that the 1992/93 event appears in both SPI3- and SMPct-based envelope curves,

but the SMPct-based pluvial event has longer duration (i.e., continues to March 1994) likely due to soil moisture memory. European drought envelope curves are dominated by the top three largest droughts [Table S1 and Fig. 6; for example, the 1953/54 event covering central Europe (Briffa et al. 1994) and the 1970s event over British Islands and central Europe (Green 1977; Hannaford et al. 2011)], whose maximum spatial coverage can reach to 75%. As for pluvials, the envelope curves consist of more spatially disconnected events that span a smaller extent compared to droughts. Notable pluvials include the most severe episode over the United Kingdom during 2012/13 (Kendon and McCarthy 2015) and a more recent (2015/16) episode across the United Kingdom and Ireland (McCarthy et al. 2016). In Asia, the most spatially extensive drought (1975–77) occurred over Kazakhstan and western Russia (Kazhydromet 2006; Schubert et al. 2014), which is also the longest, contributing to the tail of the envelopes. The longest and largest pluvial identified in this region occurs more recently (2012–16; Table S1), but this event contributes to the envelope curve only at very small extent. The majority of the pluvial severity envelopes are made up of the 1966/67 event over northern Russia and 2000–02 (the second largest) pluvial over Kazakhstan (Ta et al. 2018). According to the SAD envelope curve in South America, the fourth largest drought (2015/16; Jiménez-Muñoz et al. 2016; Erfanian et al. 2017) is also the most severe one for almost all the 3- and 6-month droughts. Interestingly, the longest-duration meteorological pluvial (1973–75) dominates almost the entire SAD envelope curves for all durations, occurring at similar locations compared to the 1973/74 agricultural type pluvial (Fig. 8). In Africa, the largest and longest meteorological droughts all occur during the 1980s and 1990s (consistent with those agricultural droughts), among which the top three largest ones (two in 1983/1984, 1991/1992) dominate the envelopes. Similarly, pluvial envelope curves are dominated by the top two longest (1961/62, 1967/68) and largest (1961/62, 1951/52) (Hoerling et al. 2006) episodes. Compared to other continents, severe droughts and pluvials in Oceania have much larger spatial extent, which can cover up to 90% of the total continents. The 1965 and 2002/03 droughts (Mpelasoka et al. 2008) dominate 3- and 9-month envelope curves, respectively, whereas points on the pluvial envelope curves come almost entirely from the largest and longest pluvial (1973/74).

Agricultural droughts and pluvials. In North America, the 1950s drought (1951–59, Cook et al. 1999; Sheffield et al. 2009) dominate the 6- and 9-month SAD envelope curves, especially for larger spatial extents (covering most of Canada and the central United States), whereas the 1968–71 drought over northeastern United States and 1976/77 drought over central Canada and the northern United States (Cook et al. 1999; Keyantash and Dracup 2004) are the most severe for smaller extents and shorter durations. For pluvials, most severe episodes occurring in the 1980s dominate the envelope curves. For example, the 1981–84 pluvial is the worst for large extents up to 50% fraction (covering the Great Plains, the western United States, and Canada), whereas the 1984–89 pluvial is the worst for smaller extents. Note the almost identical pluvial envelopes for 3- and 6-month durations, which indicates that the 6-month events remain at high severity as they propagate. In Europe, the 1953/54 drought (over much of central Europe) is the most severe for 3-month duration (Briffa et al. 1994). Almost at the same time (1952–54), a severe pluvial event occurred over northwestern Europe, which dominates a large proportion of the 3- and 6-month SAD envelope curves. Pluvials that occurred during recent periods (e.g., 2012/13 and 1998/99) over northern Europe are the most spatially extensive, with coverage up to 60% of the total area. Different from other continents, drought and pluvial envelope curves of Asia are generally inseparable and cover a much smaller fraction with much steeper slopes. Part of this could be due to the large size of the continent, which has more variable climate and land surface conditions that allow droughts and pluvials to split more easily and rapidly and potentially more difficult to persist. Notable events include the 1983–87 Siberian drought (Sheffield et al. 2009) and 2007/08 droughts over Middle East

(Trigo et al. 2010; Barlow et al. 2016) and northern China, which dominate the SAD envelope curves for smaller and larger extents, respectively. Following the 1983–87 drought, wet conditions lead to an almost 5-yr (1987–91) pluvial covering northern China (Qian and Zhu 2001; Qian et al. 2003), central Mongolia and central Russia. Although this pluvial does not have the longest duration (Table S1), it is the most severe one in Asia for both smaller and larger extents. In South America, the latest 2015/16 Amazon drought (Jiménez-Muñoz et al. 2016; Erfanian et al. 2017) dominates the envelope curve for all durations, especially for large extents. A 7-month drought that occurred in 1985 has the highest severity among all the short-duration and small-extent events. For pluvials, the envelope curves are made up of more individual episodes in this continent, especially for smaller events. For larger extents, the 1973/74 pluvial over Peru, northern Brazil and Argentina (Compagnucci et al. 2002) dominates the 6- and 9-month SAD curves. In Africa, droughts are dominated by events that occurred in the 1980s and 1990s, with the 1984/85 drought (Tarhule and Lamb 2003; Dai et al. 2004a; Sheffield et al. 2009; Zhan et al. 2016) being the most severe one across almost the full range of spatial extent and for almost all durations. In contrast, severe pluvials in this continent mainly occurred over the Sahel during early 1950s (Folland et al. 1986) and over central Africa during the 1960s–70s (Laraque et al. 2001). Compared to other continents, Oceania has the smallest slope of severity for both pluvials and droughts, but with the largest possible spatial extent up to ~80% (although this is relative to the arid and semi-arid conditions across much of the continent). Dominant and widespread droughts mainly occur in the 1960s (White et al. 2003; Mpelasoka et al. 2008), whereas the widespread 1973/74 pluvial (Plummer et al. 1999) contributes almost the entire envelope curve.

Univariate risk analysis of droughts and pluvials. We use run theory to estimate the frequency of drought and pluvial events with different duration categories (short and medium term) and generate both agricultural-type (based on SMPct; Fig. 9) and meteorological-type (based on SPI3; Fig. S14) global hazard maps (represented by return periods). Overall, the spatial distribution of event occurrence is similar between droughts and pluvials, albeit with slight local differences, indicating a general equal frequency of these two extremes

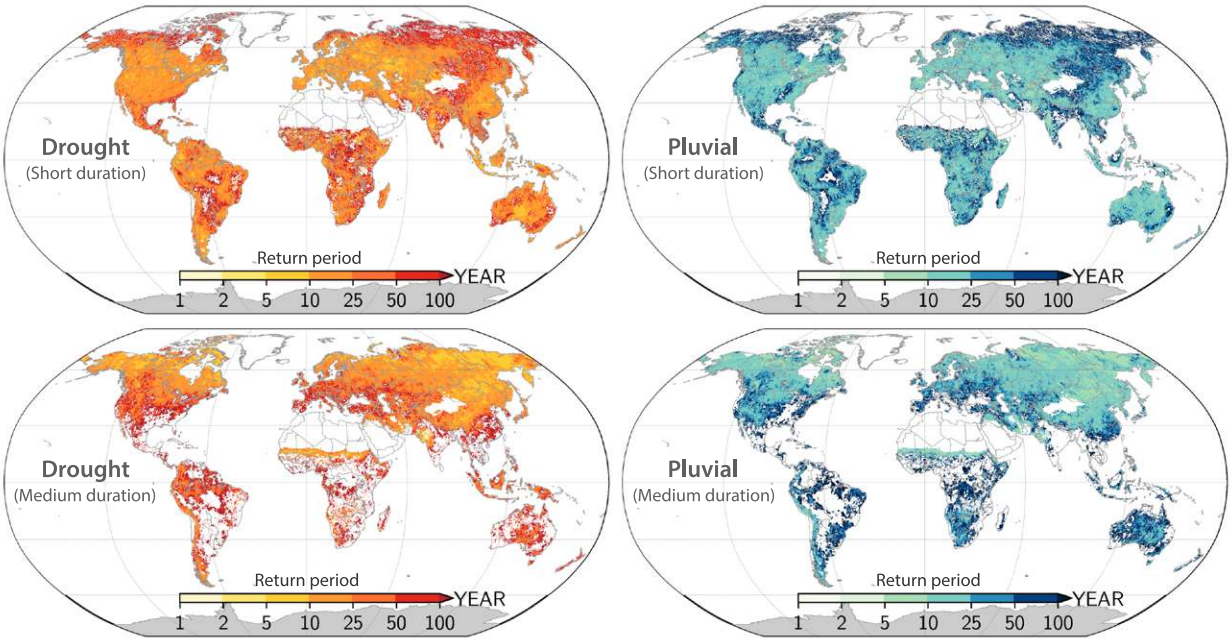

Fig. 9. Maps showing the return period of large-scale (left) drought and (right) pluvial events with (top) short-term (4–6 months) and (bottom) medium-term (7–12 months) duration based on SMPct.

over a long period (about seven decades), which is consistent with previous regional studies (e.g., Bhalme and Mooley 1980). This pattern is within our expectation as event indices have been standardized and the thresholds (below 20%/above 80%) that define droughts/pluvials are symmetrical. Differences will occur spatially and between drought and pluvial because of differences in the temporal characteristics of individual events. We find that short-duration agricultural-type droughts and pluvials occur more frequently than medium-duration events over North America, Europe, Central Asia, Southeast China, the northwestern part of South America, southern Africa, and central Australia, where climate is more variable. In contrast, high-frequency, medium-duration droughts and pluvials based on SMPct are mainly found over high latitudes, including northern Canada and Siberia, due to persistent anomalies of soil moisture in cold seasons because of freezing temperatures. These medium-duration agricultural extremes also have high frequency over northeastern and central China, the Sahel, and the western Andes. Such spatial heterogeneity of event frequency is less captured in SPI3-based analysis, highlighting the important role and necessity of accounting for the filtering processes of the land surface in drought and flood/pluvial hazard assessment.

Multivariate risk analysis of droughts and pluvials. As properties of droughts/pluvials are inherently and stochastically correlated, frequency analysis should consider their coupled characteristics (i.e., severity, area, and duration) and heterogeneous dependence structures within a suitable multivariate setting, instead of using the conventional univariate framework. From the risk assessment perspective, this is important because not accounting for the multivariate nature of these extremes can lead to an underestimation of their combined impact. To avoid this, we perform probabilistic copula analysis (see appendix B, section "Copula-based risk analysis") to estimate the joint return period of paired properties of severity and area, and focus on medium-duration (≥6 months) droughts/pluvials since these events may have larger impact on water resources management. This enables us to quantify drought and pluvial risks as well as to accommodate their commonalities and differences in a probabilistic and consistent way. We use two examples over Africa (Fig. 10) and North America (Fig. S15) to illustrate the importance of considering the dependence structure of event characteristics for risk assessment. Strong asymmetric and tail dependence is evident, where data points are clustered toward the upper-left corner (high severity but small extent, especially in Fig. S15). As droughts/pluvials become more spatially extensive, the dependence between severity and area decreases due to increased spatial variability of soil moisture. Such reduced correlation leads to a wider spread of level curves between different return periods (RPs), especially in North America (Fig. S15). Differences in RP-level curves also exist between SMPct- and SPI3-based analysis, indicating that meteorological and agricultural types of extremes have different risks even for events with the same severity, area, and duration. This further reinforces the necessity to consider the joint dependence structure between different variables and for different types of extremes. Results show that SMPct-based RP-level curves are generally higher than those based on SPI3, which means agricultural extremes have smaller return periods than meteorological extremes given the same magnitude of severity and area. This implies a higher likelihood of occurrence for agricultural extremes and therefore higher risks, because of the strong dependence between SMPct-based severity and spatial extent, which is likely due to the soil moisture memory effect. Similar analysis can be applied to examine how risk differs between droughts and pluvials. In Africa, pluvials have a lower likelihood of occurrence compared to droughts as can be seen from the downward shift of pluvial RP-level curves (Fig. 10). However, such a difference is subtle in North America (Fig. S15), indicating commensurate risks between droughts and pluvials.

The joint frequency analysis indicates that it is not necessary for all characteristics of droughts/pluvials to be extreme such that their compound impact is extreme. For instance, the 1990/91 meteorological drought in Africa (Fig. 10b) is not the most severe one if risk is assessed based on either severity or area independently. However, the joint return period of this drought is larger than 100 years indicating a low probability (less than 0.01) of occurrence if severity and area are considered simultaneously. Considering such compound impact, the 1961/62, 1973/74, and 1976 pluvials (Fig. 10c) are exceptional with no historical precedent in their severity and area extent. Such events, on average, should occur within an interval of more than 100 years. But, in reality, they occur within a time period of 15 years and therefore

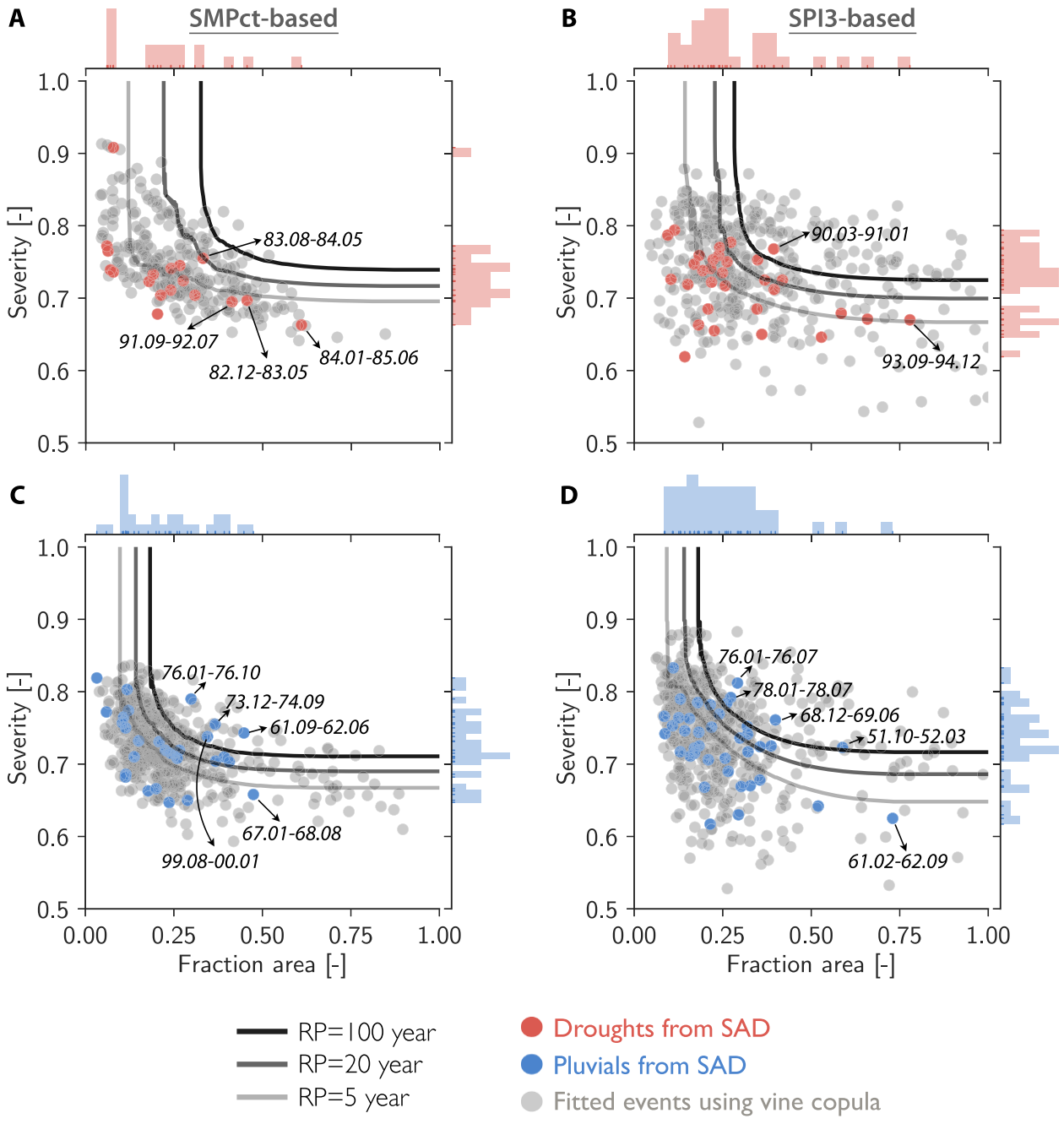

Fig. 10. African (a),(b) droughts and (c),(d) pluvials detected from SAD (red and blue colors) and randomly permuted through vine copula (gray color) based on (left) SMPct and (right) SPI3. Isolines denote the conditional bivariate return periods (i.e., 5, 20, 100 years) showing a set of possible realizations of area and severity that share the same probability. All events have a minimum duration of 6 months.

may cause more devastating impact. Similar pairs of events (1976 and 1978 pluvials) are also identified based on SPI3 (Fig. 10d). This situation can be even worse if exceptional droughts and pluvials follow each other over a short period of time, which can magnify the impact of individual drought or pluvial events, and puts more pressure on emergency preparedness and disaster response. For instance, the exceptional 1988 pluvial in North America (Fig. S15d) occurred on the back of the continent's exceptional 1987 drought, challenging water resources planning and management especially for reservoir operations.

Summary and discussion

This study provides a new panoptic view of both pixel-level and event-level drought and flood (pluvial and fluvial) risks through the development of the Global Drought and Flood Catalogue (GDFC). The GDFC is developed based on enhanced global hydrological model simulations with new meteorological forcings (PGFv3), new model processes (VIC and CaMa-Flood), and higher spatial resolution (0.25°). Datasets in the GDFC are analyzed to quantify the spatial–temporal characteristics (including severity, spatial extent, and duration) of large-scale drought and pluvial events with a particular focus on characterizing the long-term trend and variability in risk from both univariate and multivariate perspectives. Additional fluvial (inundation and streamflow) risk maps are also included in the GDFC (see details in the first section and Figs. S16 and S17 in the supplemental material). It should be noted that our estimates are focused on large-scale dry and wet extremes and by no means capture small-scale flooding (e.g., as compiled by the Dartmouth Flood Observatory; Brakenridge 2019). Nevertheless, this Catalogue facilitates our understanding of the changing behavior of these hydrologic extremes and can be used for analysis of individual events, their drivers and impacts, risk assessment of different types of events, and as a benchmark for model evaluation. Here we only focus on the hazard component of risk, but this is a fundamental component of the full-impact risk assessment that also incorporates vulnerability and exposure. The following findings are worthy of emphasis and exploration in future work.

Commonalities and differences between droughts and pluvials. Although numerous studies exist on drought and flood risk, most of them treat drought and flood separately. Development of the GDFC enables the study of the commonalities and differences between these two types of extremes in a comprehensive and systematic way. At the pixel level, we find that long-term drought and pluvial frequency have symmetric spatial patterns, which is mainly due to the definition of extremes, although geographical difference exists. At the event level, the stationarity of drought and pluvial occurrence is more complex, depending on the index type (whether precipitation driven or soil moisture driven), event duration (short term vs long term), and geographical location. Globally, the occurrence rate of short-term meteorological droughts has decreased significantly, while there is no robust trend detected for short-term meteorological pluvials. Agricultural type droughts and pluvials tend to be more temporally coherent with a dampened decadal variability compared to meteorological extremes. Through a large sample of individual drought and pluvial episodes, we are able to examine whether droughts are statistically different from pluvials in terms of area and severity, although conclusions vary across continents. Further consideration of the joint dependence among the multivariate characteristics (i.e., severity, area, and duration) indicates that both droughts and pluvials have strong and asymmetric dependence between severity and areal extent. Given the same compound impact (e.g., same magnitude of severity and area), pluvials have a lower chance of occurrence than droughts in Africa, but such difference is subtle in North America. These diagnostic findings together with a large number of event-based drought and pluvial episodes in the GDFC can enable a more detailed analysis through case studies to advance

our understanding of the underlying physical mechanisms that drive the occurrence and changes in these extremes.

Challenges and future directions. The impact of drought and flood hazards on societies is large and is likely to further intensify under anthropogenic climate change and future human activities. Reducing impacts requires bridging the gap between large-scale hazard mapping and local-scale impact assessment, and integrating this with the knowledge and activities of users on the ground, including water resources managers and meteorological, hydrological, and disaster response agencies. The interface of these agencies and region-specific management objectives could enable the diverse use of the GFDC in decision-making and impact assessment. For instance, disaster response agencies could map the GDFC hazard information to the management space that is more relevant to reservoir managers' decision-making, such as flood risk management, water supply, and hydropower generation. From the long-term-planning perspective, decision-makers can take historic records in the GDFC to examine whether existing engineering design (e.g., reservoir storage based on previous estimated return periods) could withstand future droughts and floods with increased frequency and magnitude. Such evaluation could guide government's investment decisions to reduce future impacts by enhancing the resilience of current water infrastructure. In addition, better understanding is needed of hazard-impact linkages and the scale differences between this study and impacts on the ground (He et al. 2019). To promote actionable science and support decision making across scales, information such as from the GDFC needs to be integrated in the form of scalable and policy relevant Catalogue databases accounting for human influences. This is challenging and efforts to achieve this are at early stages, but a promising avenue is to harness recent advances in hyperresolution land surface modeling (Wood et al. 2011), high-resolution satellite remote sensing (Sheffield et al. 2018), data downscaling techniques (e.g., Maraun et al. 2010; He et al. 2016), and human–water interaction analysis (e.g., He et al. 2017; Wada et al. 2017), and to incorporate this into the existing seamless monitoring and predicting systems (e.g., Sheffield et al. 2014). However, case studies need to be carefully designed to better understand the potential of generalizing such integrated frameworks to large scales.

In this study, we focus on large-scale and long-term droughts and floods, as these hydrological extremes tend to have a much larger societal impact, compared to traditional small-scale and short-duration events. This is also limited by our modeling platform, in which VIC and CaMa-Flood are designed for hydrological simulations at large basin/floodplain scales, rather than small streams, lakes, and estuaries. Therefore, the GDFC should be applied with caution for floods if risk is to be assessed at local scale and short duration (e.g., a few hours) such as flash flooding. Further combination of the hazard information with local exposure and vulnerability information can provide a more complete picture of risk and the associated impact. This is also valuable for developing adaptation and mitigation strategies to withstand future elevated drought and flood risk and improve society's resilience, if more individual and/or multiple pair-event case studies (Kreibich et al. 2017) are conducted. Such efforts can reveal general and transferable conclusions for both developed and developing countries, which have different coping capacities to droughts and floods even when they experience hazards of the same magnitude. Moreover, continued efforts are needed to incorporate the dynamic nature of drought and flood risk (e.g., how risks evolve in time) into the current static GDFC, so that future adaptation strategies can be designed in an adaptive way. It should be noted that current GDFC only provides deterministic information on drought and flood risk, but would benefit from incorporating understanding of uncertainties so that risk information can be utilized to identify strategies that are robust to a wide range of possible future scenarios (Hall et al. 2012). Quantifying such uncertainties is challenging, especially when accounting for uncertainties from different sources. This requires an improved understanding of known

and unknown physical processes related to drought and flood mechanisms (e.g., Sivapalan et al. 2005; Sheffield et al. 2012; Zhao et al. 2017), and whether current land surface models are suitable to simulate these processes within the full picture of the hydrological cycle, for example, not only focusing on streamflow and soil moisture simulation, but also on the role of terrestrial storage (e.g., Döll et al. 2014; Livneh and Hoerling 2016) or water management (e.g., He et al. 2017). Some of these aspects have been examined previously for the VIC model specifically, indicating that uncertainties in hydrological extremes tend to be dominated by the model structure, especially over snow-dominated and arid regions (e.g., Sheffield and Wood 2007; Sheffield et al. 2012; Lin et al. 2019), where physical processes related to snow (e.g., Sheffield et al. 2003; Pan et al. 2003; Xia et al. 2018) and evapotranspiration partitioning (e.g., Bohn and Vivoni 2016) are not well understood, and other key hydrological processes (e.g., groundwater dynamics, irrigation) are missing. Therefore, risk information compiled in the GDFC should be interpreted with caution over regions where these processes are important. There are other factors that make uncertainty quantification even challenging but worth exploring in future work. One of them is related to the quality (e.g., availability, coverage) of observational datasets, which are either used as input forcings to drive land surface models (such as precipitation data), or adopted to parameterize certain hydrological processes (e.g., soil properties data), or utilized for calibration and validation purposes (e.g., streamflow data). Uncertainties are likely higher in regions such as Africa where observational constraints on the model simulations are fewer. Future studies are warranted to explore this aspect and examine to what degree risk quantification is dependent on the quality and richness of these observations through regional comparisons (e.g., North America vs Africa). Nevertheless, one potential and emerging approach to tackle these issues is through ensemble frameworks, where scenarios with multiple forcings (e.g., Biemans et al. 2009; Müller Schmied et al. 2016), multiple land surface models (e.g., Nijssen et al. 2014; Dankers et al. 2014; Prudhomme et al. 2014; Samaniego et al. 2018), and multiple parameterizations schemes (e.g., Wood et al. 1998; Zaherpour et al. 2018) can be combined together to explore the full spectrum of uncertainties of drought and flood risk.

Acknowledgments. The authors gratefully acknowledge funding from NOAA Grant NA14OAR4310218, and the Mary and Randall Hack '69 Research Fund from the Princeton Environmental Institute at Princeton University, without which this study could not have taken place. This work was also funded through the 'Building REsearch Capacity for sustainable water and food security In drylands of sub-saharan Africa' (BRECcIA) which is supported by UK Research and Innovation as part of the Global Challenges Research Fund Grant NE/P021093/1.

Appendix A: Enhanced hydrologic data

Enhanced global meteorological forcings. We have developed an updated and extended v3 of the meteorological forcing dataset, PGF (Sheffield et al. 2006), from 1948 to 2016 at 3-hourly temporal resolution and 0.25° spatial resolution. PGF is a hybrid dataset of meteorological data derived from the National Centers for Environmental Prediction (NCEP)–National Center for Atmospheric Research (NCAR) reanalysis and a suite of global observation-based products. Compared to the original PGF, precipitation in PGFv3 is scaled to match updated monthly products of the Climate Research Unit (CRU) TS3.24 that has fixed some of the wet biases observed in earlier versions (Trenberth et al. 2014). Corrections are also made to the reanalysis rain-day statistics that have been found to exhibit a spurious wavelike pattern in high-latitude wintertime (Sheffield et al. 2004b). Precipitation is disaggregated in space to 0.25° by statistical downscaling using relationships developed with the GPCP (Adler et al. 2003) daily product. Disaggregation in time from daily to 3 hourly is accomplished similarly, using the TRMM Multisatellite Precipitation Analysis (TMPA) 3-hourly real-time dataset. Other

meteorological variables (downward longwave radiation, specific humidity, and surface air pressure) are downscaled in space accounting for changes in elevation. Surface air temperature is scaled to match the CRU dataset in terms of monthly means and diurnal range. The reanalysis downward shortwave and longwave radiation products are adjusted for systematic bias using the NASA Langley Research Center Surface Radiation Budget (SRB) remote sensing–based dataset (Gupta et al. 1999) and spurious trends in the shortwave radiation are corrected using relationships with cloud cover. These data are available online (http://hydrology.princeton.edu/data/hexg/GDFC).

Enhanced land surface model simulations. The VIC (Liang et al. 1994, 1996; Cherkauer et al. 2003) land surface model (LSM) is utilized for the offline simulation of the terrestrial water cycle over the period 1948–2016 covering the global land area except for Antarctica. Over the past few decades, VIC has been widely used to understand statistical characteristics and underlying physics of hydrological extremes (e.g., droughts, floods, wet extremes) from regional to global scales (e.g., Pan et al. 2013; Sheffield et al. 2014; Livneh and Hoerling 2016; Zhan et al. 2016; Samaniego et al. 2018; Lin et al. 2019). Moreover, it has been demonstrated that VIC has similar performance compared to other LSMs according to recent intermodel comparisons (e.g., Prudhomme et al. 2014; Samaniego et al. 2018). In this study, we use version 4.0.5 of VIC (an older but parallelized version), and run it in a water balance mode with a daily time step at a 0.25° spatial resolution. The model is forced with daily precipitation, maximum and minimum temperature, and wind speed obtained from the above updated PGF meteorological data. The VIC model requires a number of distributed parameter datasets as input. These include physical soil and vegetation parameters as well as a number of model specific parameters that generally require calibration. These parameters were taken from existing global simulations (Sheffield and Wood 2008a), which used parameters that were calibrated to large-basin streamflow observations. In this study, values of these parameters have been updated to take advantage of the recent SoilGrids global dataset of soil texture and properties (Hengl et al. 2014) and using new-generation pedotransfer functions (Tóth et al. 2015). The distribution of vegetation cover is taken from the Advanced Very High Resolution Radiometer (AVHRR)-based, 1-km, global land-cover dataset of Hansen et al. (2000), which uses the University of Maryland (UMD) classification scheme, by calculating the fractional area of each vegetation type within each 0.25° grid cell. Vegetation parameters such as height and stomatal resistance are specified for each of 12 vegetation classes and are taken from Nijssen et al. (2001). Values of leaf area index (LAI) are specified for each vegetation type that exists in each grid cell by resampling the dataset of Myneni et al. (1997), which is based on AVHRR normalized difference vegetation index values. The LAI values are specified for each month but do not vary from year to year. We are currently in the process of updating these to the latest MODIS-based land classifications and to use the interannually varying Global Inventory Monitoring and Modeling System (GIMMS)-AVHRR LAI dataset, and incorporating a new global depth to bedrock datasets (Shangguan et al. 2017). Three soil layers were specified, which is the usual configuration for the current version of the VIC model: a thin top layer from which soil evaporation occurs, the thicker second layer is the main soil water storage layer, and a third layer from which base flow is generated. Following Nijssen et al. (2001), the layer thicknesses were initially specified as 0.3 and 0.7 m for the first and second layers, respectively. The third-layer thickness is taken from interpolated calibrated values from previous global model simulations (Sheffield and Wood 2007) and is generally between 0.25 and 4 m. The land–sea mask and gridcell elevations are taken from the National Geophysical Data Center (NGDC) ETOPO 2-min global elevation and bathymetry dataset (U.S. Department of Commerce 2006). The elevations are also used to define the elevation subgrid tiling used in the VIC model.

Enhanced routing model. The physically based hydrodynamic model CaMa-Flood (Yamazaki et al. 2011) is utilized in this study to simulate continental-scale river discharge and flood inundation. CaMa-Flood offers several distinct advantages over existing routing models (e.g., Lohmann et al. 1998) due to its explicit representation of flood stage (e.g., water level and inundation area) in addition to river discharge for each grid cell, and more realistic hydrodynamic processes (e.g., backwater effects, bifurcation channels), yet still maintains high computational efficiency through the discretization of the entire river network into unit catchments. River network maps and flow direction maps in CaMa-Flood are generated by the Flexible Location of Waterway (FLOW; Yamazaki et al. 2009) algorithm using high-resolution hydrography datasets including HydroSHEDS for below 60°N and Global Drainage Basin Dataset (GDBD; Masutomi et al. 2009) for above 60°N. Flow direction has been modified to be consistent with a satellite-based river width dataset [Global Width Database of Large Rivers (GWD-LR); Yamazaki et al. 2014] and is used to derive the floodplain elevation profile. CaMa-Flood calculates river discharge and flow velocity using the local inertial equation proposed by Bates et al. (2010) and is forced by gridded daily runoff simulated from VIC LSM at the 0.25° spatial resolution. Floodplain inundation in CaMa-Flood is approximated at the unit-catchment scale through a subgrid parameterization scheme, which constructs a relationship between the inundation area and water level based on the floodplain elevation profile. Model spinup is repeated twice with the same year (1948) of runoff forcing to reach steady state conditions. We exclude the first two years (1948–49) from the analysis to avoid any spurious effects.

Appendix B: Statistical and risk analysis

Standardized indices. We identify large-scale hydrological extremes from both meteorological and agricultural perspectives based on two widely used indices: standardized precipitation index (SPI; WMO 2012) and SMPct (Sheffield et al. 2004a). SPI measures the standard departure of precipitation from the long-term climatology for an aggregated period (e.g., monthly, seasonal, annual). Calculation of SPI involves two steps. The first step is to fit precipitation time series at each grid cell with a gamma distribution:

$$f(P;\alpha,\beta)=\frac{\beta^{\alpha}P^{\alpha-1}e^{-\beta P}}{\Gamma(\alpha)},$$

where P is the running series of aggregated precipitation; α is the shape parameter and β is the scale parameter, both of which can be estimated through the maximum likelihood estimation (MLE) method; $\Gamma(\cdot)$ is the gamma function. The second step is to transform the cumulative probability of the fitted gamma distribution to a standard normal distribution (with mean zero and variance one). For an observed P at a given time scale, SPI is calculated as the number of standard deviations away from the median P with negative and positive values representing precipitation deficit and surplus, respectively. Following the widely used classification category (McKee et al. 1993), we define drought and large-scale flood (also referred to as pluvial) at a grid cell if the SPI is below or above the threshold of –1.0 and 1.0, respectively. Despite the advantage of convenient computation, the SPI only reflects one part of the land surface hydrologic cycle (i.e., precipitation) and ignores other important hydrologic processes including evapotranspiration (ET) and runoff (R). Soil moisture (SM)-based indices can complement this, as SM reflects the aggregated behavior of land surface water balance among P, ET, and R, and is closely related to agricultural activities (e.g., plant growth) (Sheffield et al. 2009). We estimate daily SM over the entire soil column based on VIC simulations, average it to a monthly time scale and calculate SMPct at each grid after fitting an empirical distribution.

Transforming SM into a percentile space enables us to compare the deficit and surplus of SM relative to its seasonal climatology across locations with different climate conditions (Sheffield et al. 2004a). A threshold of 20th percentile is used to define drought conditions, as suggested by the U.S. Drought Monitor. On the flip side and analogous to large-scale wet extremes, pluvials are defined in a conceptual way for grid cells with SMPct exceeding the 80th-percentile threshold.

Run theory to estimate drought and pluvial frequency. We use run theory to estimate the event (drought or pluvial) frequency at the pixel level (Yevjevich 1972; Sheffield and Wood 2007) for different duration classes D_c, which are defined as follows:

$$D_{4-6},\ \underset{4\le D\le 6}{\text{short term}}:\begin{cases}\text{SI}\le \text{SI}_0^D & \text{for drought}\\ \text{SI}\ge \text{SI}_0^P & \text{for pluvial}\end{cases},$$

$$D_{7-12},\ \underset{7\le D\le 12}{\text{medium term}}:\begin{cases}\text{SI}\le \text{SI}_0^D & \text{for drought}\\ \text{SI}\ge \text{SI}_0^P & \text{for pluvial}\end{cases},$$

where SI is the standardized index (either SPI or SMPct; see details in the previous section), and SI_0^D and SI_0^P is the event threshold for drought and pluvial, respectively. We count the total number of runs (defined as consecutive time series of SI below and above the threshold SI_0^D and SI_0^P for drought and pluvial, respectively) in the study period (1950–2016) to calculate the frequency of occurrence for short- (D_{4-6}) and medium-term (D_{7-12}) duration events. We then inverse the frequency to get the corresponding return periods.

Clustering algorithm for drought and pluvial identification. We implement an existing and well-tested approach for tracking spatially contiguous drought and pluvial events and quantifying their characteristics in time and space based on the severity–area–duration (SAD) algorithm (e.g., Andreadis et al. 2005; Sheffield et al. 2009; Zhan et al. 2016). SAD has the advantage of tracking how each individual event cluster merges or breaks at each time step. It links multivariate event characteristics (i.e., severity, spatial extent, duration) through the following equation:

$$S=1-\frac{\sum \text{SI}}{D},\quad \text{SI}\in\{\text{SPI},\text{SMPct}\},$$

where S is severity, SI is the standardized index (either SPI or SMPct; see details in appendix B, "Standardized indices" section) that defines hydrological extremes (e.g., drought or pluvial), and D is the duration in months. At each time step, the maximum spatial extent is calculated by repeatedly adding surrounding pixels with a constant increment (80 model pixels) to the center of the cluster until all contiguous pixels exceeding the threshold are included (see details in Andreadis et al. 2005; Sheffield et al. 2009). For a given duration, the maximum severity under each spatial extent forms the SAD curve. The upper bound delineated from all SAD curves forms the SAD envelope curve, which characterizes the event severity over an area given the specified duration. Two critical thresholds have to be predefined in SAD to identify the spatial clusters, including the index threshold to detect the pixel-level extremes (see details in "Standardized indices" section) and a minimum cluster size threshold N_{grids} to ensure a reasonable number of spatially connected pixels. In this study, we set N_{grids} to be 150 grids (approximately 3.75×10^5 km^2), a value suggested by the original SAD algorithm (Andreadis et al. 2005) and is recently tested by Zhan et al. (2016).

Stationarity of drought and pluvial events. We estimate the time-varying occurrence rate λ_t of drought and pluvial events through a nonparametric Gaussian kernel technique (Mudelsee et al. 2003; Mudelsee 2014) based on the following equation:

$$\lambda = \frac{1}{h}\sum_{i}^{N} K\left(\frac{t - T_i}{h}\right),$$

where h is the bandwidth, T_i is the occurrence date for the event (drought or pluvial) i (i = 1, 2, 3, ..., N), and K is the Gaussian kernel to weigh the observed event dates. We select a bandwidth of 10 years for kernel smoothing to reflect the decadal variability. To reduce the bias of estimating λ_t near boundaries, we generate pseudodata outside of the original time series with a time interval of 3 h for both left and right boundaries, yet still maintain the same empirical distribution based on the "reflection" rules suggested by Cowling and Hall (1996). Confidence intervals of λ_t are estimated using a bootstrap technique by randomly sampling the event occurrence dates 2,000 times with replacement. We calculate the Cox–Lewis statistic (Mudelsee et al. 2003) to test whether λ_t exhibits a monotonic trend with the null hypothesis of constant λ_t over the study period (1950–2016).

Copula-based risk analysis. Risk assessment of droughts and pluvials can be greatly enhanced if the dependence structure of severity S, area A, and duration D can be well represented. However, such high dimensional dependence modeling becomes inflexible due to the "curse of dimensionality." In addition, dependence structures between different pairs of variables can be very different. For instance, one pair may have tail dependence (extreme dependence) and other pairs may have symmetric or asymmetric dependence. Recent development of vine copulas (pair-copula constructions) can overcome these limitations as it can decompose the multivariate copulas into pair copulas based on hierarchical graphical models (Bedford and Cooke 2002; Kurowicka and Cooke 2006; Cooke et al. 2015). Given these advantages, the vine copula has been widely applied in hydrology recently (e.g., Hao and Singh 2016; Wanders et al. 2017; Bevacqua et al. 2017). In this study, we utilized the R package VineCopula to optimize the vine structure (either C-vine or D-vine) through the determination of the most appropriate bivariate copula family and its corresponding parameters (see details in Schepsmeier et al. 2012). We test seven parametric distributions (exponential, gamma, generalized extreme value, generalized Pareto, lognormal, Weibull minimum, and Weibull maximum) to find the most suitable fit of the marginal distribution for S, A, and D. As D is discrete (integer values with the unit of month) and has repeated values (called "ties"), the rank of data points is not unique anymore, making the multivariate analysis ambiguous (e.g., the fit of the marginal distribution). To overcome this issue, we add random noise (called "jittering") to the original discrete datasets and generate 200 continuous pseudosamples following the procedures suggested by De Michele et al. (2013). For each random sample, we first identify the best-fitted distribution and count how many times each distribution is selected. The distribution with the highest selection frequency is then identified as the best-fitted distribution for D. After fitting the three-dimensional joint distribution function using the vine copula, the joint nonexceedance probability between S and A conditional on D can be calculated as

$$\begin{aligned} p_{SA|D} &:= \mathbb{P}\left[S > s, A > a \middle| D > d\right] \\ &= 1 - F\left(S \le s, A \le a \middle| D > d\right) \\ &= 1 - \frac{C_{SA}\left(u_s, u_a\right) - C_{SAD}\left(u_s, \boldsymbol{u}_a, u_d\right)}{1 - u_d}, \end{aligned} \tag{B1}$$

where u_s, u_a, $u_d = F_S(s)$, $F_A(a)$, and $F_D(d)$ are marginal distributions for S, A, and D; C_{SA} and C_{SAD} are copula functions fitted from the vine copula. Different from the conventional univariate RP, here we calculate the so-called Kendall's return period (KRP) $T_{SA|D}$, to ensure the mathematical consistency for multivariate events as suggested by Salvadori et al. (2011):

$$T_{SA|D} = \frac{\mu}{1 - \overline{K_C}(\bar{q})}, \tag{B2}$$

where $\mu = N/n$ is the average interarrival time; N is the number of years; n is the number of events, $\overline{K_C}(\bar{q}) := \mathbb{P}\left[p_{SA|D} \geq \bar{q} \right]$ is the Kendall's survival function, and $\bar{q}$ is the survival Kendall's quantile. For any return period $T_{SA|D}$ (e.g., 100 years), $\bar{q}$ can be calculated through the inversion of $\overline{K_C}$ from Eq. (B2):

$$\bar{q} = \overline{K_C}^{-1}\left(1 - \frac{\mu}{T_{SA|D}}\right). \tag{B3}$$

Substitute $\bar{q}$ into Eq. (B1) and calculate the quantiles of S and A based on their marginal distributions, we can get a bundle of isolines, which represent a combination of realizations of S and A that share the same RPs (Salvadori et al. 2013).

References

Abel, G. J., M. Brottrager, J. C. Cuaresma, and R. Muttarak, 2019: Climate, conflict and forced migration. *Global Environ. Change*, **54**, 239–249, https://doi.org/10.1016/j.gloenvcha.2018.12.003.

Adams, C., T. Ide, J. Barnett, and A. Detges, 2018: Sampling bias in climate–conflict research. *Nat. Climate Change*, **8**, 200–203, https://doi.org/10.1038/s41558-018-0068-2.

Adler, R. F., and Coauthors, 2003: The version-2 Global Precipitation Climatology Project (GPCP) monthly precipitation analysis (1979–present). *J. Hydrometeor.*, **4**, 1147–1167, https://doi.org/10.1175/1525-7541(2003)004<1147:TVGPCP>2.0.CO;2.

AghaKouchak, A., and N. Nakhjiri, 2012: A near real-time satellite-based global drought climate data record. *Environ. Res. Lett.*, **7**, 044037, https://doi.org/10.1088/1748-9326/7/4/044037.

Andreadis, K. M., E. A. Clark, A. W. Wood, A. F. Hamlet, and D. P. Lettenmaier, 2005: Twentieth-century drought in the conterminous United States. *J. Hydrometeor.*, **6**, 985–1001, https://doi.org/10.1175/JHM450.1.

Arnell, N. W., and S. N. Gosling, 2016: The impacts of climate change on river flood risk at the global scale. *Climatic Change*, **134**, 387–401, https://doi.org/10.1007/s10584-014-1084-5.

Barlow, M., B. Zaitchik, S. Paz, E. Black, J. Evans, and A. Hoell, 2016: A review of drought in the Middle East and southwest Asia. *J. Climate*, **29**, 8547–8574, https://doi.org/10.1175/JCLI-D-13-00692.1.

Bates, P. D., M. S. Horritt, and T. J. Fewtrell, 2010: A simple inertial formulation of the shallow water equations for efficient two-dimensional flood inundation modelling. *J. Hydrol.*, **387**, 33–45, https://doi.org/10.1016/j.jhydrol.2010.03.027.

Bedford, T., and R. M. Cooke, 2002: Vines—A new graphical model for dependent random variables. *Ann. Stat.*, **30**, 1031–1068, https://doi.org/10.1214/AOS/1031689016.

Bevacqua, E., D. Maraun, I. Hobæk Haff, M. Widmann, and M. Vrac, 2017: Multivariate statistical modelling of compound events via pair-copula constructions: Analysis of floods in Ravenna (Italy). *Hydrol. Earth Syst. Sci.*, **21**, 2701–2723, https://doi.org/10.5194/hess-21-2701-2017.

Bhalme, H. N., and D. A. Mooley, 1980: Large-scale droughts/floods and monsoon circulation. *Mon. Wea. Rev.*, **108**, 1197–1211, https://doi.org/10.1175/1520-0493(1980)108<1197:LSDAMC>2.0.CO;2.

Biemans, H., R. Hutjes, P. Kabat, B. Strengers, D. Gerten, and S. Rost, 2009: Effects of precipitation uncertainty on discharge calculations for main river basins. *J. Hydrometeor.*, **10**, 1011–1025, https://doi.org/10.1175/2008JHM1067.1.

Bierkens, M. F., 2015: Global hydrology 2015: State, trends, and directions. *Water Resour. Res.*, **51**, 4923–4947, https://doi.org/10.1002/2015WR017173.

Black, R., W. N. Adger, N. W. Arnell, S. Dercon, A. Geddes, and D. Thomas, 2011: The effect of environmental change on human migration. *Global Environ. Change*, **21**, S3–S11, https://doi.org/10.1016/j.gloenvcha.2011.10.001.

Bohn, T. J., and E. R. Vivoni, 2016: Process-based characterization of evapotranspiration sources over the North American monsoon region. *Water Resour. Res.*, **52**, 358–384, https://doi.org/10.1002/2015WR017934.

Brakenridge, G. R., 2019: Global active archive of large flood events. Dartmouth Flood Observatory, accessed 6 January 2019, www.dartmouth.edu/~floods/Archives/index.html.

Briffa, K., P. Jones, and M. Hulme, 1994: Summer moisture variability across Europe, 1892–1991: An analysis based on the Palmer drought severity index. *Int. J. Climatol.*, **14**, 475–506, https://doi.org/10.1002/joc.3370140502.

Cherkauer, K. A., L. C. Bowling, and D. P. Lettenmaier, 2003: Variable infiltration capacity cold land process model updates. *Global Planet. Change*, **38**, 151–159, https://doi.org/10.1016/S0921-8181(03)00025-0.

Compagnucci, R., E. Agosta, and W. Vargas, 2002: Climatic change and quasi-oscillations in central-west Argentina summer precipitation: Main features and coherent behaviour with southern African region. *Climate Dyn.*, **18**, 421–435, https://doi.org/10.1007/s003820100183.

Cook, E. R., D. M. Meko, D. W. Stahle, and M. K. Cleaveland, 1999: Drought reconstructions for the continental United States. *J. Climate*, **12**, 1145–1162, https://doi.org/10.1175/1520-0442(1999)012<1145:DRFTCU>2.0.CO;2.

Cooke, R. M., D. Kurowicka, and K. Wilson, 2015: Sampling, conditionalizing, counting, merging, searching regular vines. *J. Multivar. Anal.*, **138**, 4–18, https://doi.org/10.1016/j.jmva.2015.02.001.

Cottrell, R. S., and Coauthors, 2019: Food production shocks across land and sea. *Nat. Sustainability*, **2**, 130–137, https://doi.org/10.1038/s41893-018-0210-1.

Cowling, A., and P. Hall, 1996: On pseudodata methods for removing boundary effects in kernel density estimation. *J. Roy. Stat. Soc.*, **58B**, 551–563, https://doi.org/10.1111/j.2517-6161.1996.tb02100.x.

Dai, A., 2011: Drought under global warming: A review. *Wiley Interdiscip. Rev.: Climate Change*, **2**, 45–65, https://doi.org/10.1002/WCC.81.

——, P. J. Lamb, K. E. Trenberth, M. Hulme, P. D. Jones, and P. Xie, 2004a: The recent Sahel drought is real. *Int. J. Climatol.*, **24**, 1323–1331, https://doi.org/10.1002/joc.1083.

——, K. E. Trenberth, and T. Qian, 2004b: A global dataset of Palmer drought severity index for 1870–2002: Relationship with soil moisture and effects of surface warming. *J. Hydrometeor.*, **5**, 1117–1130, https://doi.org/10.1175/JHM-386.1.

Dankers, R., and Coauthors, 2014: First look at changes in flood hazard in the Inter-Sectoral Impact Model Intercomparison Project ensemble. *Proc. Natl. Acad. Sci. USA*, **111**, 3257–3261, https://doi.org/10.1073/pnas.1302078110.

De Michele, C., G. Salvadori, R. Vezzoli, and S. Pecora, 2013: Multivariate assessment of droughts: Frequency analysis and dynamic return period. *Water Resour. Res.*, **49**, 6985–6994, https://doi.org/10.1002/wrcr.20551.

Diem, J. E., S. J. Ryan, J. Hartter, and M. W. Palace, 2014: Satellite-based rainfall data reveal a recent drying trend in central equatorial Africa. *Climatic Change*, **126**, 263–272, https://doi.org/10.1007/s10584-014-1217-x.

Döll, P., M. Fritsche, A. Eicker, and H. M. Schmied, 2014: Seasonal water storage variations as impacted by water abstractions: Comparing the output of a global hydrological model with GRACE and GPS observations. *Surv. Geophys.*, **35**, 1311–1331, https://doi.org/10.1007/s10712-014-9282-2.

EM-DAT, 2018: The international disaster database. Université Catholique de Louvain, accessed 20 October 2018, www.emdat.be/.

Erfanian, A., G. Wang, and L. Fomenko, 2017: Unprecedented drought over tropical South America in 2016: Significantly under-predicted by tropical SST. *Sci. Rep.*, **7**, 5811, https://doi.org/10.1038/s41598-017-05373-2.

European Union, 2007: On the assessment and management of flood risks. Directive 2007/60/EC, 116 pp.

Evans, G. W., 2019: Projected behavioral impacts of global climate change. *Annu. Rev. Psychol.*, **70**, 449–474, https://doi.org/10.1146/annurev-psych-010418-103023.

Feng, S., A. B. Krueger, and M. Oppenheimer, 2010: Linkages among climate change, crop yields and Mexico–US cross-border migration. *Proc. Natl. Acad. Sci. USA*, **107**, 14257–14262, https://doi.org/10.1073/pnas.1002632107.

Fernandez, A., J. Black, M. Jones, L. Wilson, L. Salvador-Carulla, T. Astell-Burt, and D. Black, 2015: Flooding and mental health: A systematic mapping review. *PLOS ONE*, **10**, e0119929, https://doi.org/10.1371/journal.pone.0119929.

Field, C. B., 2012: *Managing the Risks of Extreme Events and Disasters to Advance Climate Change Adaptation*. Cambridge University Press, 592 pp.

Fluet-Chouinard, E., B. Lehner, L.-M. Rebelo, F. Papa, and S. K. Hamilton, 2015: Development of a global inundation map at high spatial resolution from topographic downscaling of coarse-scale remote sensing data. *Remote Sens. Environ.*, **158**, 348–361, https://doi.org/10.1016/j.rse.2014.10.015.

Folland, C. K., T. N. Palmer, and D. E. Parker, 1986: Sahel rainfall and worldwide sea temperatures, 1901–85. *Nature*, **320**, 602–607, https://doi.org/10.1038/320602a0.

Ghimire, R., S. Ferreira, and J. H. Dorfman, 2015: Flood-induced displacement and civil conflict. *World Dev.*, **66**, 614–628, https://doi.org/10.1016/j.worlddev.2014.09.021.

Gleick, P. H., 2014: Water, drought, climate change, and conflict in Syria. *Wea. Climate Soc.*, **6**, 331–340, https://doi.org/10.1175/WCAS-D-13-00059.1.

Goddard, L., 2016: From science to service. *Science*, **353**, 1366–1367, https://doi.org/10.1126/science.aag3087.

Green, J., 1977: The weather during July 1976: Some dynamical considerations of the drought. *Weather*, **32**, 120–126, https://doi.org/10.1002/j.1477-8696.1977.tb04532.x.

Guillod, B. P., B. Orlowsky, D. G. Miralles, A. J. Teuling, and S. I. Seneviratne, 2015: Reconciling spatial and temporal soil moisture effects on afternoon rainfall. *Nat. Commun.*, **6**, 6443, https://doi.org/10.1038/ncomms7443.

Gupta, S. K., N. A. Ritchey, A. C. Wilber, C. H. Whitlock, G. G. Gibson, and P. W. Stackhouse Jr., 1999: A climatology of surface radiation budget derived from satellite data. *J. Climate*, **12**, 2691–2710, https://doi.org/10.1175/1520-0442(1999)012<2691:ACOSRB>2.0.CO;2.

Haigh, T., and Coauthors, 2018: Provision of climate services for agriculture: Public and private pathways to farm decision-making. *Bull. Amer. Meteor. Soc.*, **99**, 1781–1790, https://doi.org/10.1175/BAMS-D-17-0253.1.

Haines, A., R. S. Kovats, D. Campbell-Lendrum, and C. Corvalán, 2006: Climate change and human health: Impacts, vulnerability and public health. *Public Health*, **120**, 585–596, https://doi.org/10.1016/j.puhe.2006.01.002.

Hajat, S., K. Ebi, R. Kovats, B. Menne, S. Edwards, and A. Haines, 2005: The human health consequences of flooding in Europe: A review. *Extreme Weather Events and Public Health Responses*, W. Kirch et al., Eds., Springer, 185–196.

Hall, J. W., R. J. Lempert, K. Keller, A. Hackbarth, C. Mijere, and D. J. McInerney, 2012: Robust climate policies under uncertainty: A comparison of robust decision making and info-gap methods. *Risk Anal.*, **32**, 1657–1672, https://doi.org/10.1111/j.1539-6924.2012.01802.x.

Hannaford, J., B. Lloyd-Hughes, C. Keef, S. Parry, and C. Prudhomme, 2011: Examining the large-scale spatial coherence of European drought using regional indicators of precipitation and streamflow deficit. *Hydrol. Processes*, **25**, 1146–1162, https://doi.org/10.1002/hyp.7725.

Hansen, M. C., R. S. DeFries, J. R. Townshend, and R. Sohlberg, 2000: Global land cover classification at 1 km spatial resolution using a classification tree approach. *Int. J. Remote Sens.*, **21**, 1331–1364, https://doi.org/10.1080/014311600210209.

Hao, Z., and V. P. Singh, 2016: Review of dependence modeling in hydrology and water resources. *Prog. Phys. Geogr.*, **40**, 549–578, https://doi.org/10.1177/0309133316632460.

——, A. AghaKouchak, N. Nakhjiri, and A. Farahmand, 2014: Global integrated drought monitoring and prediction system. *Sci. Data*, **1**, 140001, https://doi.org/10.1038/SDATA.2014.1.

——, V. Singh, and F. Hao, 2018: Compound extremes in hydroclimatology: A review. *Water*, **10**, 718, https://doi.org/10.3390/W10060718.

Haraguchi, M., and U. Lall, 2015: Flood risks and impacts: A case study of Thailand's floods in 2011 and research questions for supply chain decision making. *Int. J. Disaster Risk Reduct.*, **14**, 256–272, https://doi.org/10.1016/j.ijdrr.2014.09.005.

He, X., N. W. Chaney, M. Schleiss, and J. Sheffield, 2016: Spatial downscaling of precipitation using adaptable random forests. *Water Resour. Res.*, **52**, 8217–8237, https://doi.org/10.1002/2016WR019034.

——, Y. Wada, N. Wanders, and J. Sheffield, 2017: Intensification of hydrological drought in California by human water management. *Geophys. Res. Lett.*, **44**, 1777–1785, https://doi.org/10.1002/2016GL071665.

——, L. Estes, M. Konar, D. Tian, D. Anghileri, K. Baylis, T. P. Evans, and J. Sheffield, 2019: Integrated approaches to understanding and reducing drought impact on food security across scales. *Curr. Opin. Environ. Sustainability*, **40**, 43–54, https://doi.org/10.1016/j.cosust.2019.09.006.

Heim, R. R., Jr., and M. J. Brewer, 2012: The Global Drought Monitor Portal: The foundation for a global drought information system. *Earth Interact.*, **16**, https://doi.org/10.1175/2012EI000446.1.

Hengl, T., and Coauthors, 2014: SoilGrids1km——Global soil information based on automated mapping. *PLOS ONE*, **9**, e105992, https://doi.org/10.1371/JOURNAL.PONE.0105992.

Herold, C., F. Mouton, K. Verdin, J. Verdin, R. Brackenridge, Z. Liu, A. Tyagi, and G. Wolfgang, 2011: Floods. Appendix 1: Global risk analysis, Global Assessment Rep. 2009, 11–16, www.preventionweb.net/english/hyogo/gar/appendices/documents/Appendix-1.doc.

Hewitt, C., S. Mason, and D. Walland, 2012: The Global Framework For Climate Services. *Nat. Climate Change*, **2**, 831–832, https://doi.org/10.1038/nclimate1745.

Hirabayashi, Y., R. Mahendran, S. Koirala, L. Konoshima, D. Yamazaki, S. Watanabe, H. Kim, and S. Kanae, 2013: Global flood risk under climate change. *Nat. Climate Change*, **3**, 816–821, https://doi.org/10.1038/nclimate1911.

Hoerling, M., J. Hurrell, J. Eischeid, and A. Phillips, 2006: Detection and attribution of twentieth-century northern and southern African rainfall change. *J. Climate*, **19**, 3989–4008, https://doi.org/10.1175/JCLI3842.1.

in den Bäumen, H. S., J. Toebben, and M. Lenzen, 2015: Labour forced impacts and production losses due to the 2013 flood in Germany. *J. Hydrol.*, **527**, 142–150, https://doi.org/10.1016/J.JHYDROL.2015.04.030.

IPCC, 2018: *Global Warming of 1.5°C*. World Meteorological Organization, 32 pp.

Ji, L., P. Gong, J. Wang, J. Shi, and Z. Zhu, 2018: Construction of the 500-m resolution daily global surface water change database (2001–2016). *Water Resour. Res.*, **54**, 10 270–10 292, https://doi.org/10.1029/2018WR023060.

Jiménez-Muñoz, J. C., C. Mattar, J. Barichivich, A. Santamaría-Artigas, K. Takahashi, Y. Malhi, J. A. Sobrino, and G. Van Der Schrier, 2016: Record-breaking warming and extreme drought in the Amazon rainforest during the course of El Niño 2015–2016. *Sci. Rep.*, **6**, 33130, https://doi.org/10.1038/srep33130.

Kazhydromet, 2006: Drought management and mitigation assessment for Kazakhstan, phase two: Regional vulnerability and capacity assessment survey. Kazakhstan Nature Protection Ministry Rep., 196 pp., http://siteresources.worldbank.org/EXTECAREGTOPRURDEV/Resources/573581-1164120557290/KazakstanDroughtPlan-English.pdf.

Kelley, C. P., S. Mohtadi, M. A. Cane, R. Seager, and Y. Kushnir, 2015: Climate change in the Fertile Crescent and implications of the recent Syrian drought. *Proc. Natl. Acad. Sci. USA*, **112**, 3241–3246, https://doi.org/10.1073/pnas.1421533112.

Kendon, M., and M. McCarthy, 2015: The UK's wet and stormy winter of 2013/2014. *Weather*, **70**, 40–47, https://doi.org/10.1002/wea.2465.

Keyantash, J. A., and J. A. Dracup, 2004: An aggregate drought index: Assessing drought severity based on fluctuations in the hydrologic cycle and surface water storage. *Water Resour. Res.*, **40**, W09304, https://doi.org/10.1029/2003WR002610.

King-Okumu, C., B. Jillo, J. Kinyanjui, and I. Jarso, 2018: Devolving water governance in the Kenyan arid lands: From top-down drought and flood emergency response to locally driven water resource development planning. *Int. J. Water Resour. Dev.*, **34**, 675–697, https://doi.org/10.1080/07900627.2017.1357539.

Kreibich, H., and Coauthors, 2017: Adaptation to flood risk: Results of international paired flood event studies. *Earth's Future*, **5**, 953–965, https://doi.org/10.1002/2017EF000606.

Kurowicka, D., and R. M. Cooke, 2006: *Uncertainty Analysis with High Dimensional Dependence Modelling.* John Wiley and Sons, 284 pp.

Laraque, A., G. Mahé, D. Orange, and B. Marieu, 2001: Spatiotemporal variations in hydrological regimes within central Africa during the XXth century. *J. Hydrol.*, **245**, 104–117, https://doi.org/10.1016/S0022-1694(01)00340-7.

Leonard, M., and Coauthors, 2014: A compound event framework for understanding extreme impacts. *Wiley Interdiscip. Rev.: Climate Change*, **5**, 113–128, https://doi.org/10.1002/WCC.252.

Lettenmaier, D. P., D. Alsdorf, J. Dozier, G. J. Huffman, M. Pan, and E. F. Wood, 2015: Inroads of remote sensing into hydrologic science during the WRR era. *Water Resour. Res.*, **51**, 7309–7342, https://doi.org/10.1002/2015WR017616.

Liang, X., D. P. Lettenmaier, E. F. Wood, and S. J. Burges, 1994: A simple hydrologically based model of land surface water and energy fluxes for general circulation models. *J. Geophys. Res.*, **99**, 14 415–14 428, https://doi.org/10.1029/94JD00483.

——, E. F. Wood, and D. P. Lettenmaier, 1996: Surface soil moisture parameterization of the VIC-2L model: Evaluation and modification. *Global Planet. Change*, **13**, 195–206, https://doi.org/10.1016/0921-8181(95)00046-1.

Liebmann, B., and Coauthors, 2014: Understanding recent eastern Horn of Africa rainfall variability and change. *J. Climate*, **27**, 8630–8645, https://doi.org/10.1175/JCLI-D-13-00714.1.

Lin, P., and Coauthors, 2019: Global reconstruction of naturalized river flows at 2.94 million reaches. *Water Resour. Res.*, **55**, 6499–6516, https://doi.org/10.1029/2019WR025287.

Livneh, B., and M. P. Hoerling, 2016: The physics of drought in the U.S. central Great Plains. *J. Climate*, **29**, 6783–6804, https://doi.org/10.1175/JCLI-D-15-0697.1.

Lloyd-Hughes, B., C. Prudhomme, J. Hannaford, S. Parry, C. Keef, and G. Rees, 2009: The spatial coherence of European droughts: UK and Europe drought catalogues. Environment Agency Sci. Rep. SC070079/SR, 64 pp., http://nora.nerc.ac.uk/8615/1/SC070079_EA_SR1_EuropeanDroughtCatalogue.pdf.

Lohmann, D., E. Raschke, B. Nijssen, and D. Lettenmaier, 1998: Regional scale hydrology: I. Formulation of the VIC-2L model coupled to a routing model. *Hydrol. Sci. J.*, **43**, 131–141, https://doi.org/10.1080/02626669809492107.

Mach, K. J., and Coauthors, 2019: Climate as a risk factor for armed conflict. *Nature*, **571**, 193–197, https://doi.org/10.1038/s41586-019-1300-6.

Maraun, D., and Coauthors, 2010: Precipitation downscaling under climate change: Recent developments to bridge the gap between dynamical models and the end user. *Rev. Geophys.*, **48**, RG3003, https://doi.org/10.1029/2009RG000314.

Masutomi, Y., Y. Inui, K. Takahashi, and Y. Matsuoka, 2009: Development of highly accurate global polygonal drainage basin data. *Hydrol. Processes*, **23**, 572–584, https://doi.org/10.1002/hyp.7186.

Maystadt, J.-F., and O. Ecker, 2014: Extreme weather and civil war: Does drought fuel conflict in Somalia through livestock price shocks? *Amer. J. Agric. Econ.*, **96**, 1157–1182, https://doi.org/10.1093/ajae/aau010.

McCarthy, M., S. Spillane, S. Walsh, and M. Kendon, 2016: The meteorology of the exceptional winter of 2015/2016 across the UK and Ireland. *Weather*, **71**, 305–313, https://doi.org/10.1002/wea.2823.

McKee, T. B., N. J. Doesken, and J. Kleist, 1993: The relationship of drought frequency and duration to time scales. *Proc. Eighth Conf. on Applied Climatology*, Anaheim, CA, Amer. Meteor. Soc., 179–183.

Milly, P. C. D., R. T. Wetherald, K. Dunne, and T. L. Delworth, 2002: Increasing risk of great floods in a changing climate. *Nature*, **415**, 514–517, https://doi.org/10.1038/415514a.

Miralles, D. G., P. Gentine, S. I. Seneviratne, and A. J. Teuling, 2019: Land–atmospheric feedbacks during droughts and heatwaves: State of the science and current challenges. *Ann. N. Y. Acad. Sci.*, **1436**, 19–35, https://doi.org/10.1111/nyas.13912.

Moftakhari, H. R., G. Salvadori, A. AghaKouchak, B. F. Sanders, and R. A. Matthew, 2017: Compounding effects of sea level rise and fluvial flooding. *Proc. Natl. Acad. Sci. USA*, **114**, 9785–9790, https://doi.org/10.1073/pnas.1620325114.

Mora, C., and Coauthors, 2018: Broad threat to humanity from cumulative climate hazards intensified by greenhouse gas emissions. *Nat. Climate Change*, **8**, 1062–1071, https://doi.org/10.1038/s41558-018-0315-6.

Mpelasoka, F., K. Hennessy, R. Jones, and B. Bates, 2008: Comparison of suitable drought indices for climate change impacts assessment over Australia towards resource management. *Int. J. Climatol.*, **28**, 1283–1292, https://doi.org/10.1002/joc.1649.

Mudelsee, M., 2014: Bootstrap confidence intervals. *Climate Time Series Analysis: Classical Statistical and Bootstrap Methods*, Springer, 65–112.

——, M. Börngen, G. Tetzlaff, and U. Grünewald, 2003: No upward trends in the occurrence of extreme floods in central Europe. *Nature*, **425**, 166–169, https://doi.org/10.1038/nature01928.

Müller Schmied, H., and Coauthors, 2016: Variations of global and continental water balance components as impacted by climate forcing uncertainty and human water use. *Hydrol. Earth Syst. Sci.*, **20**, 2877–2898, https://doi.org/10.5194/hess-20-2877-2016.

Myneni, R. B., R. Ramakrishna, R. Nemani, and S. W. Running, 1997: Estimation of global leaf area index and absorbed PAR using radiative transfer models. *IEEE Trans. Geosci. Remote Sens.*, **35**, 1380–1393, https://doi.org/10.1109/36.649788.

Nijssen, B., R. Schnur, and D. P. Lettenmaier, 2001: Global retrospective estimation of soil moisture using the variable infiltration capacity land surface model, 1980–93. *J. Climate*, **14**, 1790–1808, https://doi.org/10.1175/1520-0442(2001)014<1790:GREOSM>2.0.CO;2.

——, S. Shukla, C. Lin, H. Gao, T. Zhou, J. Sheffield, E. F. Wood, and D. P. Lettenmaier, 2014: A prototype global drought information system based on multiple land surface models. *J. Hydrometeor.*, **15**, 1661–1676, https://doi.org/10.1175/JHM-D-13-090.1.

Orlowsky, B., and S. I. Seneviratne, 2013: Elusive drought: Uncertainty in observed trends and short- and long-term CMIP5 projections. *Hydrol. Earth Syst. Sci.*, **17**, 1765–1781, https://doi.org/10.5194/hess-17-1765-2013.

Pal, J. S., and E. A. Eltahir, 2002: Teleconnections of soil moisture and rainfall during the 1993 Midwest summer flood. *Geophys. Res. Lett.*, **29**, 1865, https://doi.org/10.1029/2002GL014815.

Pall, P., T. Aina, D. A. Stone, P. A. Stott, T. Nozawa, A. G. Hilberts, D. Lohmann, and M. R. Allen, 2011: Anthropogenic greenhouse gas contribution to flood risk in England and Wales in autumn 2000. *Nature*, **470**, 382–385, https://doi.org/10.1038/nature09762.

Palmer, M. A., D. P. Lettenmaier, N. L. Poff, S. L. Postel, B. Richter, and R. Warner, 2009: Climate change and river ecosystems: Protection and adaptation options. *Environ. Manage.*, **44**, 1053–1068, https://doi.org/10.1007/s00267-009-9329-1.

Pan, M., and Coauthors, 2003: Snow process modeling in the North American Land Data Assimilation System (NLDAS): 2. Evaluation of model simulated snow water equivalent. *J. Geophys. Res.*, **108**, 8850, https://doi.org/10.1029/2003JD003994.

——, X. Yuan, and E. F. Wood, 2013: A probabilistic framework for assessing drought recovery. *Geophys. Res. Lett.*, **40**, 3637–3642, https://doi.org/10.1002/grl.50728.

Pappenberger, F., E. Dutra, F. Wetterhall, and H. L. Cloke, 2012: Deriving global flood hazard maps of fluvial floods through a physical model cascade. *Hydrol. Earth Syst. Sci.*, **16**, 4143–4156, https://doi.org/10.5194/hess-16-4143-2012.

Perch-Nielsen, S. L., M. B. Bättig, and D. Imboden, 2008: Exploring the link between climate change and migration. *Climatic Change*, **91**, 375, https://doi.org/10.1007/s10584-008-9416-y.

Plummer, N., and Coauthors, 1999: Changes in climate extremes over the Australian region and New Zealand during the twentieth century. *Climatic Change*, **42**, 183–202, https://doi.org/10.1023/A:1005472418209.

Prudhomme, C., and Coauthors, 2014: Hydrological droughts in the 21st century, hotspots and uncertainties from a global multimodel ensemble experiment. *Proc. Natl. Acad. Sci. USA*, **111**, 3262–3267, https://doi.org/10.1073/pnas.1222473110.

Qian, W., and Y. Zhu, 2001: Climate change in China from 1880 to 1998 and its impact on the environmental condition. *Climatic Change*, **50**, 419–444, https://doi.org/10.1023/A:1010673212131.

——, Q. Hu, Y. Zhu, and D.-K. Lee, 2003: Centennial-scale dry-wet variations in East Asia. *Climate Dyn.*, **21**, 77–89, https://doi.org/10.1007/s00382-003-0319-3.

Salvadori, G., F. Durante, and C. De Michele, 2011: On the return period and design in a multivariate framework. *Hydrol. Earth Syst. Sci.*, **15**, 3293–3305, https://doi.org/10.5194/hess-15-3293-2011.

——, ——, and ——, 2013: Multivariate return period calculation via survival functions. *Water Resour. Res.*, **49**, 2308–2311, https://doi.org/10.1002/wrcr.20204.

Samaniego, L., and Coauthors, 2018: Anthropogenic warming exacerbates European soil moisture droughts. *Nat. Climate Change*, **8**, 421–426, https://doi.org/10.1038/s41558-018-0138-5.

Schepsmeier, U., J. Stoeber, E. C. Brechmann, B. Graeler, T. Nagler, T. Erhardt, 2012: VineCopula: Statistical inference of vine copulas, version 1. R package, https://tnagler.github.io/VineCopula/.

Schubert, S. D., H. Wang, R. D. Koster, M. J. Suarez, and P. Ya. Groisman, 2014: Northern Eurasian heat waves and droughts. *J. Climate*, **27**, 3169–3207, https://doi.org/10.1175/JCLI-D-13-00360.1.

——, and Coauthors, 2016: Global meteorological drought: A synthesis of current understanding with a focus on SST drivers of precipitation deficits. *J. Climate*, **29**, 3989–4019, https://doi.org/10.1175/JCLI-D-15-0452.1.

Seager, R., Y. Kushnir, C. Herweijer, N. Naik, and J. Velez, 2005: Modeling of tropical forcing of persistent droughts and pluvials over western North America: 1856–2000. *J. Climate*, **18**, 4065–4088, https://doi.org/10.1175/JCLI3522.1.

Seneviratne, S. I., and Coauthors, 2012: Changes in climate extremes and their impacts on the natural physical environment: An overview of the IPCC SREX report. *Geophysical Research Abstracts*, Vol. 14, Abstract 12566, https://meetingorganizer.copernicus.org/EGU2012/EGU2012-12566.pdf.

Shangguan, W., T. Hengl, J. Mendes de Jesus, H. Yuan, and Y. Dai, 2017: Mapping the global depth to bedrock for land surface modeling. *J. Adv. Model. Earth Syst.*, **9**, 65–88, https://doi.org/10.1002/2016MS000686.

Sheffield, J., and E. F. Wood, 2007: Characteristics of global and regional drought, 1950–2000: Analysis of soil moisture data from off-line simulation of the terrestrial hydrologic cycle. *J. Geophys. Res.*, **112**, D17115, https://doi.org/10.1029/2006JD008288.

——, and ——, 2008a: Global trends and variability in soil moisture and drought characteristics, 1950–2000, from observation-driven simulations of the terrestrial hydrologic cycle. *J. Climate*, **21**, 432–458, https://doi.org/10.1175/2007JCLI1822.1.

——, and ——, 2008b: Projected changes in drought occurrence under future global warming from multi-model, multi-scenario, IPCC AR4 simulations. *Climate Dyn.*, **31**, 79–105, https://doi.org/10.1007/s00382-007-0340-z.

——, and Coauthors, 2003: Snow process modeling in the North American Land Data Assimilation System (NLDAS): 1. Evaluation of model-simulated snow cover extent. *J. Geophys. Res.*, **108**, 8849, https://doi.org/10.1029/2002JD003274.

——, G. Goteti, F. Wen, and E. F. Wood, 2004a: A simulated soil moisture based drought analysis for the United States. *J. Geophys. Res.*, **109**, D24108, https://doi.org/10.1029/2004JD005182.

——, A. D. Ziegler, E. F. Wood, and Y. Chen, 2004b: Correction of the high-latitude rain day anomaly in the NCEP–NCAR reanalysis for land surface hydrological modeling. *J. Climate*, **17**, 3814–3828, https://doi.org/10.1175/1520-0442(2004)017<3814:COTHRD>2.0.CO;2.

——, G. Goteti, and E. F. Wood, 2006: Development of a 50-year high-resolution global dataset of meteorological forcings for land surface modeling. *J. Climate*, **19**, 3088–3111, https://doi.org/10.1175/JCLI3790.1.

——, K. Andreadis, E. F. Wood, and D. P. Lettenmaier, 2009: Global and continental drought in the second half of the twentieth century: Severity–area–duration analysis and temporal variability of large-scale events. *J. Climate*, **22**, 1962–1981, https://doi.org/10.1175/2008JCLI2722.1.

——, B. Livneh, and E. F. Wood, 2012: Representation of terrestrial hydrology and large-scale drought of the continental United States from the North American Regional Reanalysis. *J. Hydrometeor.*, **13**, 856–876, https://doi.org/10.1175/JHM-D-11-065.1.

——, and Coauthors, 2014: A drought monitoring and forecasting system for sub-Sahara African water resources and food security. *Bull. Amer. Meteor. Soc.*, **95**, 861–882, https://doi.org/10.1175/BAMS-D-12-00124.1.

——, E. F. Wood, M. Pan, H. Beck, G. Coccia, A. Serrat-Capdevila, and K. Verbist, 2018: Satellite remote sensing for water resources management: Potential for supporting sustainable development in data-poor regions. *Water Resour. Res.*, **54**, 9724–9758, https://doi.org/10.1029/2017WR022437.

Shen, X., Y. Mei, and E. N. Anagnostou, 2017: A comprehensive database of flood events in the contiguous United States from 2002 to 2013. *Bull. Amer. Meteor. Soc.*, **98**, 1493–1502, https://doi.org/10.1175/BAMS-D-16-0125.1.

Sivapalan, M., G. Blöschl, R. Merz, and D. Gutknecht, 2005: Linking flood frequency to long-term water balance: Incorporating effects of seasonality. *Water Resour. Res.*, **41**, W06012, https://doi.org/10.1029/2004WR003439.

Ta, Z., R. Yu, X. Chen, G. Mu, and Y. Guo, 2018: Analysis of the spatio-temporal patterns of dry and wet conditions in central Asia. *Atmosphere*, **9**, 7, https://doi.org/10.3390/atmos9010007.

Tarhule, A., and P. J. Lamb, 2003: Climate research and seasonal forecasting for West Africans: Perceptions, dissemination, and use? *Bull. Amer. Meteor. Soc.*, **84**, 1741–1760, https://doi.org/10.1175/BAMS-84-12-1741.

Tóth, B., M. Weynants, A. Nemes, A. Makó, G. Bilas, and G. Tóth, 2015: New generation of hydraulic pedotransfer functions for Europe. *Eur. J. Soil Sci.*, **66**, 226–238, https://doi.org/10.1111/ejss.12192.

Trenberth, K. E., A. Dai, G. van der Schrier, P. D. Jones, J. Barichivich, K. R. Briffa, and J. Sheffield, 2014: Global warming and changes in drought. *Nat. Climate Change*, **4**, 17–22, https://doi.org/10.1038/nclimate2067.

Trigo, R. M., C. M. Gouveia, and D. Barriopedro, 2010: The intense 2007–2009 drought in the Fertile Crescent: Impacts and associated atmospheric circulation. *Agric. For. Meteor.*, **150**, 1245–1257, https://doi.org/10.1016/j.agrformet.2010.05.006.

UNISDR, 2015: The human cost of weather related disasters. UN Office for Disaster Risk Reduction Rep., 30 pp.

U.S. Department of Commerce, 2006: 2-minute gridded global relief data (ETOPO2), version 2. NOAA National Geophysical Data Center, accessed 9 October 2017, https://data.noaa.gov/dataset/dataset/2-minute-gridded-global-relief-data-etopo2-v2.

Wada, Y., and Coauthors, 2017: Human–water interface in hydrological modelling: Current status and future directions. *Hydrol. Earth Syst. Sci.*, **21**, 4169–4193, https://doi.org/10.5194/hess-21-4169-2017.

Wanders, N., and Coauthors, 2017: Forecasting the hydroclimatic signature of the 2015–16 El Niño event on the western United States. *J. Hydrometeor.*, **18**, 177–186, https://doi.org/10.1175/JHM-D-16-0230.1.

Wang, S.-Y. S., W.-R. Huang, H.-H. Hsu, and R. R. Gillies, 2015: Role of the strengthened El Niño teleconnection in the May 2015 floods over the southern Great Plains. *Geophys. Res. Lett.*, **42**, 8140–8146, https://doi.org/10.1002/2015GL065211.

Ward, P. J., B. Jongman, F. S. Weiland, A. Bouwman, R. van Beek, M. F. Bierkens, W. Ligtvoet, and H. C. Winsemius, 2013: Assessing flood risk at the global scale: Model setup, results, and sensitivity. *Environ. Res. Lett.*, **8**, 044019, https://doi.org/10.1088/1748-9326/8/4/044019.

White, W. B., G. McKeon, and J. Syktus, 2003: Australian drought: The interference of multi-spectral global standing modes and travelling waves. *Int. J. Climatol.*, **23**, 631–662, https://doi.org/10.1002/joc.895.

WMO (2012), Standardized Precipitation Index User Guide. https://public.wmo.int/en/resources/library/standardized-precipitation-index-user-guide

Wood, E. F., and Coauthors, 1998: The Project for Intercomparison of Land-Surface Parameterization Schemes (PILPS) Phase 2(c) Red–Arkansas River basin experiment: 1. Experiment description and summary intercomparisons. *Global Planet. Change*, **19**, 115–135, https://doi.org/10.1016/S0921-8181(98)00044-7.

——, and Coauthors, 2011: Hyperresolution global land surface modeling: Meeting a grand challenge for monitoring Earth's terrestrial water. *Water Resour. Res.*, **47**, W05301, https://doi.org/10.1029/2010WR010090.

Wuebbles, D. J., D. W. Fahey, and K. A. Hibbard, 2017: Climate science special report: Fourth National Climate Assessment. Vol. I. U.S. Global Change Research Program Rep., 470 pp.

Xia, Y., and Coauthors, 2018: Comprehensive evaluation of the variable infiltration capacity (VIC) model in the North American Land Data Assimilation System. *J. Hydrometeor.*, **19**, 1853–1879, https://doi.org/10.1175/JHM-D-18-0139.1.

Yamazaki, D., T. Oki, and S. Kanae, 2009: Deriving a global river network map and its sub-grid topographic characteristics from a fine-resolution flow direction map. *Hydrol. Earth Syst. Sci.*, **13**, 2241–2251, https://doi.org/10.5194/hess-13-2241-2009.

——, S. Kanae, H. Kim, and T. Oki, 2011: A physically based description of floodplain inundation dynamics in a global river routing model. *Water Resour. Res.*, **47**, W04501, https://doi.org/10.1029/2010WR009726.

——, F. O'Loughlin, M. A. Trigg, Z. F. Miller, T. M. Pavelsky, and P. D. Bates, 2014: Development of the global width database for large rivers. *Water Resour. Res.*, **50**, 3467–3480, https://doi.org/10.1002/2013WR014664.

Yevjevich, V., 1972: *Stochastic Processes in Hydrology*. Water Resources, 276 pp.

Zaherpour, J., and Coauthors, 2018: Worldwide evaluation of mean and extreme runoff from six global-scale hydrological models that account for human impacts. *Environ. Res. Lett.*, **13**, 065015, https://doi.org/10.1088/1748-9326/AAC547.

Zhan, W., K. Guan, J. Sheffield, and E. F. Wood, 2016: Depiction of drought over sub-Saharan Africa using reanalyses precipitation data sets. *J. Geophys. Res. Atmos.*, **121**, 10 555–10 574, https://doi.org/10.1002/2016JD024858.

Zhao, F., and Coauthors, 2017: The critical role of the routing scheme in simulating peak river discharge in global hydrological models. *Environ. Res. Lett.*, **12**, 075003, https://doi.org/10.1088/1748-9326/aa7250.

Zscheischler, J., and S. I. Seneviratne, 2017: Dependence of drivers affects risks associated with compound events. *Sci. Adv.*, **3**, e1700263, https://doi.org/10.1126/SCIADV.1700263.